



Influence of Hydro-climatic Factors on Streamflow Patterns in Chilean Catchments

Alejandra A. Stehr¹, Cristóbal Benavente¹, Felipe Orellana¹

¹Department of Civil Engineering, University of Concepción, Concepción, 4030000, Chile

5 Correspondence to: Alejandra Stehr (astehr@udec.cl)

Abstract. Chile's extreme latitudinal gradient (18°-56°S) and diverse climatic regimes make it a natural laboratory for understanding hydro-climatic controls on streamflow evolution under climate change. This study quantifies maximum streamflow trends and their relationships with precipitation, temperature, and soil moisture across 38 catchments representing nine distinct Chilean climate zones over 2000-2021. We integrated field streamflow observations, gridded climate datasets (CR2MET), and satellite soil moisture data (SMAP/SMOS), applying Mann-Kendall trend analysis, Theil-Sen slope estimation, and Spearman correlation tests Results reveal significant declining streamflow trends in 67% of winter-rainfall catchments (median slope: -1.12 mm/year, p<0.1), while summer-rainfall and tundra regions show the most substantial temperature increases (+0.06°C/year). Mediterranean and temperate climates exhibit the strongest precipitation-streamflow correlations ($\rho = 0.20$ -0.79), with soil moisture acting as an intermediate control mechanism. Our findings indicate that accumulated precipitation is the dominant driver in 53% of analysed catchments, with soil moisture modulate the precipitation-runoff relationship, particularly in water-limited environments. These results provide critical insights for water resource management in Chile's diverse climatic regions and contribute to understanding hydro-climatic linkages in transitional climate zones globally.

20 1 Introduction

Climate change has a significant impact on hydrological systems worldwide, altering precipitation patterns, temperature regimes, and streamflow characteristics. Understanding these trends is crucial for effective water resource management, accurate flood risk assessment, and informed adaptation planning. Climate change can be defined as persistent variations in climate statistics over decades or longer (Gocic and Trajkovic, 2013). In recent decades, it has threatened ecosystems and increased risks for human societies through changes in the spatial and temporal patterns of seasonality, mean conditions, interannual variability, extreme events, and cryosphere dynamics, among other impacts on the biosphere and the hydrological cycle (IPCC, 2023). A central aspect of climate change is global warming, which has contributed to the more frequent occurrence of extreme climatic and hydrologic events, with negative consequences for ecosystems, economies, and human activities (Crosbie et al., 2013).



45



The continental region of Chile is particularly vulnerable to climate change because it contains unique environments and a wide variety of climatic regimes along strong latitudinal and altitudinal gradients (Madariaga Gomez de Cuenca, 2021). For example, Chile spans 38° of latitude with precipitation varying from <1mm/year in the Atacama to >3000mm/year in Patagonia. In this context, streamflow extremes and their drivers are critical variables to assess; however, recent studies have yielded diverse and sometimes contrasting results. For instance, Blöschl et al. (2019) found that in Europe, high streamflow values are generally associated with strong effects of soil moisture and winter rainfall. Do et al. (2017) used continental-scale datasets to report that annual maximum streamflow has decreased in North America, Australia, and parts of Europe, while increasing in other regions, such as eastern North America, parts of South America, and southern Africa. Their analysis by climate type indicated decreasing trends in arid, warm summer dry, warm winter dry, and snow summer dry climates, while equatorial, fully humid, snow-humid, and polar climates showed mixed responses. These findings highlight the global non-uniformity of flood peak responses and the need to account for anthropogenic influences in hydrological analyses.

In Chile, Boisier et al. (2018) documented multi-decadal declines in precipitation and streamflow across central-southern regions (30-48°S), attributing these trends primarily to anthropogenic climate change. Analysis of 106 Chilean catchments during the recent megadrought (2010-2020) revealed that snow-dominated Andean basins experience amplified streamflow deficits due to hydrological memory effects, where antecedent storage conditions modulate precipitation-runoff relationships (Álvarez-Garretón et al., 2021). These findings underscore the complexity of hydro-climatic interactions in mountainous regions with diverse storage mechanisms.

For many years, global studies primarily focused on streamflow, temperature, and precipitation. Regional investigations illustrate the heterogeneity of these trends. In Iran, Minaei and Irannezhad (2018) observed that precipitation increases at the daily scale in mountainous semi-arid regions but decreases at the monthly scale in lowlands. They also identified significant annual warming and declining daily streamflow, although annual streamflow trends remained inconclusive. In central Italy, Gentilucci and Hamed (2023) reported decreasing streamflow in mediterranean climates and increasing flows in northern Europe during winter. They also found a pronounced decrease in precipitation, an increase in evapotranspiration, and a strong correlation between precipitation and streamflow. In southern Spain, Yeste et al. (2018) confirmed these dynamics, emphasising that precipitation redistribution and seasonality strongly influence streamflow, with summer flows showing marked declines.

Regarding temperature, Wan et al. (2022) demonstrated that surface radiometric temperatures are increasing worldwide, with land surfaces warming faster than the oceans, except in some regions where local cooling occurs. In the Himalayas, Hasson et al. (2017) demonstrated that seasonal cooling during the monsoon months and warming in other seasons alter the balance between rainfall, snowmelt, and glacial runoff, with implications for runoff seasonality and its sources. In Cyprus, Myronidis



65

75

80

85



et al. (2018) identified negative trends in streamflow in mediterranean cold-winter climates, while Ashraf et al. (2020) reported that annual flows in the Indus River increase at high elevations but decrease at lower altitudes.

Other studies emphasise the dominance of climatic drivers over oceanic signals in shaping hydrological regimes. Xu et al. (2024) concluded that climate drivers exert greater influence than ocean forcings on streamflow trends, underscoring the importance of expanding the set of explanatory variables. Among these, soil moisture has received growing attention. Alam et al. (2024) demonstrated its value for predicting seasonal streamflow in snow-influenced catchments in the western United States. In Australia, Wasko and Nathan (2019) found that soil moisture is more strongly related to streamflow when flows are less dependent on precipitation. Bhatti et al. (2024) further showed that soil moisture interacts strongly and non-linearly with temperature. Collectively, these findings illustrate the need for multivariable approaches, as single-variable analyses are insufficient to capture the complexity of hydroclimatic processes. Indeed, Swain et al. (2024) emphasised that multivariate indices offer a more comprehensive framework for quantifying compound precipitation—runoff extremes, which are becoming increasingly relevant for impact assessment.

In Chile, several studies document ongoing hydroclimatic changes. Oertel et al. (2020) identified decreasing streamflow in semi-arid, mediterranean, and temperate oceanic climates, alongside increasing temperatures in semi-arid and temperate regions. Precipitation declined significantly only in mediterranean climates, where ENSO plays a strong role. Vicuña et al. (2013) found that periods of high flow in the Mataquito basin were associated with high temperatures and infrequent precipitation. Long-term analyses by Stolpe and Undurraga (2016) revealed shifts in soil moisture and temperature regimes, suggesting more frequent dry years and a potential southward expansion of xeric conditions. Using spatial clustering, Sangüesa et al. (2023) divided Chile into arid and humid regions. They concluded that streamflows are generally declining in humid regions, while no clear patterns were observed in arid regions.

The last decade has been marked by an unprecedented megadrought, further underscoring Chile's vulnerability. Alvarez-Garreton et al. (2021) demonstrated that hydrological memory through snowpack and groundwater storage plays a key role in drought propagation, with the worst-case scenario occurring when extreme meteorological droughts follow consecutive years of precipitation deficits. Baez-Villanueva et al. (2024) reaffirmed the importance of hydrological memory, emphasising that soil moisture is a stronger predictor of streamflow than of drought. They also demonstrated that streamflow droughts in central Chile are closely linked to multi-year precipitation deficits, where memory effects and climate variability give rise to complex inter-variable dynamics. Looking forward, Vásquez et al. (2024) projected that future climate zones in Chile will be dominated by hot-desert and hot-summer mediterranean types, with snowfall increasingly confined to the central Andes and the Patagonian ice fields. These results highlight the importance of considering the current Köppen–Geiger classification, which

https://doi.org/10.5194/egusphere-2025-5318 Preprint. Discussion started: 12 November 2025

© Author(s) 2025. CC BY 4.0 License.



100

105

110

EGUsphere Preprint repository

95 in Chile includes distinctive regimes such as high-altitude climates, summer-rainfall and winter-rainfall climates, and ocean-influenced zones (Sarricolea et al., 2017).

Considering this background, this study addresses three specific objectives: (1) quantify streamflow trends across Chilean climate gradients over 2000-2021, focusing on annual maximum flows in 38 catchments spanning diverse Köppen–Geiger climate zones; (2) identify dominant hydro-climatic controls on streamflow evolution by analysing relationships among streamflow, precipitation, temperature, and soil moisture variables; and (3) assess regional variations in climate-streamflow relationships to determine how different climate zones respond to hydro-climatic drivers. The analysis integrates hydrological (Q) and meteorological (precipitation, temperature) variables, along with satellite-derived soil moisture, to capture the complexity of climate–hydrology interactions across Chile's latitudinal gradient. This work seeks to contribute to water resource management, climate adaptation, and understanding of hydrological extremes in a changing climate.

2 Materials and methods

2.1 Study area

This study examines catchments spread across continental Chile, between 18.1°S and 41.5°S and 73.5°W and 68.0°w. The climatic diversity of Chile is represented through the Köppen–Geiger classification, which includes nine third-order climate types: tundra (ET), cold desert (BWk), warm-summer mediterranean (Csb), cold semi-arid (BSk), temperate oceanic (Cfb), subpolar oceanic (Cfc), cold-summer mediterranean (Csc), hot desert (BWh), and ice cap (EF) (Sarricolea et al., 2017). Sarricolea et al. (2017) adapted this scheme for Chile by incorporating elevation, coastal influence, and rainfall seasonality, yielding 25 distinct zones.

- Nine groups of neighbouring catchments were selected to represent 11 of these 25 climate zones, with a focus on climatic diversity and regional representativeness. A climate zone was included in a study area if it covered at least 10% of the zone's surface or 15% of a specific catchment. Figure 1 shows the spatial distribution of the catchments under study, while Table 1 summarises their climatic composition and area.
- The first zone (ET (w)), located in the Arica y Parinacota Region, is characterised exclusively by a tundra climate with summer rainfall. It covers 4471 km² and includes five study catchments. The mean annual precipitation over the study period was 397.27 mm. The mean temperature was 10.99 °C, with a maximum of 19.14 °C on 31 March 2003 and a minimum of 0.3 °C on 24 July 2019.



145

150

155



- 125 The second zone (ET (w) − BSk (w)), located in the Antofagasta Region, comprises a tundra climate with summer rainfall and a cold semi-arid climate with summer rainfall, covering an area of 10128 km² and including six study catchments. The mean annual precipitation over the study period was 150.08 mm. The mean temperature was 13.31 °C, with a maximum of 21.91 °C on 31 March 2012 and a minimum of −0.55 °C on 22 July 2000.
- 130 The third zone (BSk (w) ET (w)), also situated in the Antofagasta Region, features cold semi-arid and tundra climates, with summer rainfall spanning 2243 km², and comprises three study catchments. The average annual precipitation during the study period was 100.46 mm. The mean temperature was 19.12 °C, reaching a maximum of 27.49 °C on 15 February 2016 and a minimum of 3.51 °C on 22 July 2000.
- 135 The largest zone (ET BSk (s)), situated in the Atacama Region, features a combination of tundra and cold semi-arid climates, characterised by winter rainfall. It covers 35623 km² and encompasses three study catchments. Throughout the study period, the average annual precipitation was 93.46 mm. The average temperature was 15.67 °C, reaching a maximum of 22.61 °C on 18 January 2020 and a minimum of –0.29 °C on 31 July 2011.
- The fifth zone (BSk (s) ET (s) BSk (s) (i)), also located in the Coquimbo Region, exhibits a similar climate, combining the same two types with a small area of cold semi-arid climate influenced by winter rainfall under coastal effects, covering 9591 km² and including two study catchments. The average annual precipitation during the study period was 178.87 mm. The mean temperature was 14.85 °C, with the highest recorded temperature of 23.18 °C on 27 January 2017 and the lowest of –0.88 °C on 31 July 2011.

The sixth zone (BSk (s) – ET (s)) with an area of 3130 km² is situated in the Coquimbo Region. It is mainly characterised by a cold, semi-arid climate with winter rainfall, and, to a lesser extent, by a tundra climate with winter rainfall. In this case, five study catchments with sufficient data are located close to one another. The mean annual precipitation over the study period was 306.28 mm. The mean temperature was 14.53 °C, with a maximum of 24.77 °C on 5 February 2019 and a minimum of -1.64 °C on 10 July 2000.

A mediterranean zone (ET (s) – Csb (h) – Csc), in the Metropolitana Region, combines tundra climate with winter rainfall, high-altitude warm-summer Mediterranean climate with winter rainfall, and cold-summer Mediterranean climate. The mean annual precipitation over the study period was 590.25 mm. The mean temperature was 12.42 °C, with a maximum of 24.89 °C on 26 January 2019 and a minimum of –3.28 °C on 7 June 2014. It spans 766 km² with four study catchments. Another Mediterranean zone (Csb) in the La Araucanía Region is characterised exclusively by a warm-summer Mediterranean climate with winter rainfall. It covers 5678 km² and comprises seven study catchments. The mean annual precipitation over the study



165



period was 1410.78 mm. The mean temperature was 17.78 °C, with a maximum of 36.39 °C on 20 February 2002 and a minimum of 5.22 °C on 8 July 2007.

The last zone (Cfb (i) – Cfb) is found in the Los Lagos Region, where temperate rainy climates with coastal influence and temperate rainy climates prevail, covering an area of 2871 km² and including three study catchments. The mean annual precipitation over the study period was 1797.4 mm. The mean temperature was 15.56 °C, with a maximum of 34.36 °C on 4 February 2019 and a minimum of 4.32 °C on 9 September 2000.

(a) (c) BSk (s) - ET (s) (d) **ET (w)** (e) **ET (w)** - BSk (w) CLS RLEL RLJ (f) ET (s) - Csb (h) - Csc (g) BSk (s) - ET (s) - BSk (s) (i) (i) BSk (w) - ET (w) (h) Csb ŔVŤ Gauging stations Study catchments RRQC Rivers **ìRĹĽ** Climate zones

Cold semi-arid climate with
winter rainfall (BSk (s))
Cold semi-arid climate with winter rainfall
and coastal influence (BSk (s) (i))
Cold semi-arid climate ECHCH RT (k) ET - BSk (s) (j) Cfb (i) - Cfb Coid serin-land climate with summer rainfall (BSk (w))
Temperate rainy climate (Cfb)
Temperate rainy climate (ofb)
Warm summer mediterranean climate with coastal influence (Cfb (i))
Warm summer mediterranean climate with winter rainfall (Csb)
High-allitude warm summer riigh-altitude warm summer mediterranean climate with winter rainfall (Csb (h)) Cold summer mediterranean climate (Csc) Tundra climate (ET) Tundra climate with wither spinfall (ET (a)) with winter rainfall (ET (s))
Tundra climate
with summer rainfall (ET (w))





Figure 1. The study catchments are grouped by study zones and labelled according to the dominant climate zones, ordered from left to right by surface coverage percentage. Maps use Scientific Colour Maps (SCM v7). Sequential layers are shown with the Batlow palette; categorical overlays use neutral contrasts to preserve legibility (Crameri et al., 2020).

Table 1. Climatic and morphometric characterisation of catchments grouped by study zone. The catchment names correspond to the original stations' Spanish names.

Zone	Catchment		Climate zone importance			Predominant	Area	Elevation (m a.s.l)	
	Name	Abbr.	First	Second	Third	climate zones Code (%)	(km ²)	Min	Max
ET (w)	Río Desaguadero en Cotacotani	RDC	ET (w)	-	-		376	4528	6190
	Río Lauca en estancia El Lago	RLEL	ET (w)	-	-	ET (w) (99.13%)	583	4377	6245
	Canal Lauca en Sifón n°1	CLS1	ET (w)	-	-		184	4373	5336
	Río Lauca en Japu	RLJ	ET (w)	-	-		3278	3981	6273
	Río Guallatire en Guallatire	RGG	ET (w)	-	-		50	4226	5967
	Río Toconce antes represa sendos	RTARS	ET (w)	BSk (w)	-		156	3350	5623
ET (w) - BSk (w)	Río San Pedro en Parshall N°2 (BT. CHILEX)	RSPP2	ET (w)	BSk (w)	-	ET (w) (81.04%)	1250	3335	6123
	Río Salado en sifón Ayquina	RSSA	ET (w)	BSk (w)	-		807	2948	5604
	Río Salado A. J. Curti	RSAJC	ET (w)	BSk (w)	-	BSk (w) (13.78%)	527	3115	5604
	Río Loa en Vado Santa Bárbara (DOH)	RLVSB	ET (w)	BSk (w)	-	(13.7070)	5334	3005	6050
	Río Loa antes represa Lequena	RLRL	ET (w)	BSk (w)	-		2053	3323	6144
BSk	Río San Pedro en Cuchabrachi	RSPC	ET (w)	BSk (w)	BWk (w)	BSk (w) (49.45%) ET (w)	1416	2561	5838
(w) -	Canal Vilama en Vilama	CVV	ET (w)	BSk (w)	BWk (w)		363	2559	5737
ET (w)	Canal Tilomonte antes represa	CTR	BSk (w)	BWk (w)	ET (w)	(42.23%)	463	2710	4477
ET -	Río Copiapó en ciudad de Copiapó	RCCC	BSk (s)	ET	Csc	ET (42.59%)	17115	391	5790
BSk (s)	Canal Mal Paso después de bocatoma	CMPDB	ET	BSk (s)	-	BSk (s) (35.86%)	10166	541	5860
(3)	Río Copiaó en La Puerta	RCLP	ET	BSk (s)	-	(33.0070)	8343	895	5860
BSk (s) - ET (s) - BSk (s) (i)	Río Elqui en La Serena	RELS	BSk (s)	ET (s)	BSk (s) (i)	BSk (s) (44.11%) ET (s) (39.24%)	9401	19	6081
	Estero Culebrón en El Sifón	ECES	BSk (s) (i)	-	-	BSk (s) (i) (14.57%)	190	74	1217
BSk (s) - ET (s)	Río Tascadero en desembocadura	RTD	BSk (s)	ET (s)	-		241	1229	3842
	Río Mostazal en Cuestecita	RMCU	BSk (s)	ET (s)	-	BSk (s)	394	1252	4330
	Río Mostazal en Carén	RMCA	BSk (s)	ET (s)	-	(70.81%) ET (s)	640	701	4295
	Río Grande en Las Ramadas	RGLR	BSk (s)	ET (s)	-	(28.71%)	569	1396	4299
	Río Grande en Cuyano	RGC	BSk (s)	ET (s)	-		1287	904	4246





Zone	Catchment		Climate zone importance			Predominant	Area	Elevation (m a.s.l)	
	Name	Abbr.	First	Second	Third	climate zones Code (%)	(km ²)	Min	Max
ET (s) - Csb (h) - Csc	Estero Yerba Loca antes junta San Francisco	EYLSF	ET (s)	Csc	Csb (h)	ET (s) (33.36%) Csb (h)	110	1354	5439
	Río San Francisco antes junta Estero Yerba Loca	RSFEYL	ET (s)	Csc	Csb (h)		139	1517	4868
	Río Molina antes junta San Francisco	RMSF	Csb (h)	Csc	ET (s)	(32.17%) Csc (20.93%)	300	1214	5345
	Estero Arrayán en La Montosa	EALM	Csc	Csb (h)	ET (s)		217	1049	3834
Csb	Río Vergara en Tijeral	RVT	Csb	-	1		2537	62	1777
	Río Rahue en Quebrada Culén	RRQC	Csb	ı	1		671	108	729
	Río Dumo en Santa Ana	RDSA	Csb	-	1		393	276	1083
	Estero Chufquén en Chufquén	ECHCH	Csb	1	1	Csb (93.33%)	854	115	1691
	Río Lumaco en Lumaco	RLL	Csb	ı	1		853	57	1369
	Río Traiguén en Victoria	RTV	Csb	-	1		94	330	855
	Río Quino en longitudinal	RQL	Csb	1	1		277	290	1668
Cfb (i) - Cfb	Río Negro en Las Lomas	RNLL	Cfb (i)	-	-	Cfb (i)	253	57	312
	Río Maullín en Las Quemas	RMLQ	Cfb (i)	Cfb	ı	(76.73%)	2278	17	2068
	Río Toro en Tegualda	RTT	Cfb (i)	-	-	Cfb (12.9%)	339	93	357

2.2 Data sources

- 175 The study focuses on identifying trends and correlations in extreme hydrological events. Accordingly, the variables of interest correspond to the annual maxima of streamflow, and the potential drivers are precipitation, temperature, and soil moisture. All variables were aggregated to the catchment scale, with temporal resolutions varying according to the original datasets. The study period extends from 2000 to 2021, ensuring data availability for all variables.
- Historical streamflow data were obtained from the National Water Agency (Dirección General de Aguas (DGA), 2025). A total of 38 gauging stations were considered (Fig. 1), each with continuous records covering most of the study period. To adequately capture extreme events, the highest temporal resolution available was used: hourly instantaneous discharge values. These data provide a robust characterisation of annual peak flows, which are critical for assessing hydrological extremes. Gridded precipitation and temperature data were retrieved from the CR2MET dataset (Boisier, 2023). CR2MET employs a statistical downscaling and interpolation framework that integrates ground-based observations with large-scale atmospheric reanalysis to produce spatially and temporally consistent climate fields across Chile. The product spans 1960–2021, with a spatial resolution of 0.05° (~5 km) and a daily temporal resolution. For this study, grid cells intersecting each catchment were extracted and aggregated to catchment-scale time series. This procedure ensures spatial representativeness while retaining



205

210

215



local climatic variability. Finally, soil moisture data were obtained from the Global Land Data Assimilation System version 2.1 (GLDAS-2.1; NASA GES DISC, 2020) (Rodell et al., 2004; Vicente, 2005). GLDAS combines ground observations, satellite retrievals, and advanced land-surface models (including NOAH 2.7.1) to produce globally consistent estimates of land-surface variables. The product provides coverage from 2000 to the present, with a temporal resolution of three hours and a spatial resolution of 0.25°. For each catchment, soil moisture values were extracted from intersecting grid cells and subsequently aggregated to the catchment scale. These data complement hydro-meteorological records by offering insights into subsurface storage and antecedent wetness conditions.

For all gridded datasets, catchment-scale averages were calculated by weighting grid cells based on the proportion of their area within each catchment boundary. This procedure minimises bias introduced by partial coverage of pixels along catchment borders and ensures comparability between datasets of different spatial resolutions.

200 2.3 Data processing and analytical methods

2.3.1 Variable definition and derivation

The variables of interest include annual maximum streamflow, precipitation, temperature, and soil moisture, together with derived indices that capture short-term persistence in precipitation and soil moisture. Specifically, the indices are the sevenday accumulated precipitation (PP7, Eq. 1), the three-day averaged soil moisture (SM3, Eq. 2), and the seven-day averaged soil moisture (SM7, Eq. 3). These indices are defined as follows:

$$PP7_{daily,i} = \sum_{j=i-6}^{i} PP7_{dily,j} \tag{1}$$

$$SM3_{daily,i} = \frac{1}{24} * \sum_{m=0}^{23} SM_{3h}(t_i - m)$$
 (2)

$$SM7_{daily.i} = \frac{1}{56} * \sum_{m=0}^{55} SM_{3h} (t_i - m)$$
 (3)

The PP7_{daily,i} corresponds to the sum of daily precipitation over a seven-day moving window; SM3_{daily,i} and SM7_{daily,i} are computed as moving averages of three hourly soil moisture values over three- and seven-day windows, respectively. In the three equations (Eq. 1–3), i denotes the daily time step, while j and m represent backward lags in days used in the summation windows for precipitation and soil moisture, respectively.

Catchment-scale series for precipitation, temperature, and soil moisture were obtained by spatially aggregating gridded products within each of the 38 study catchments. The aggregation was performed as area-weighted means (Eq. 4).



220

245



$$\frac{\sum_{i=1}^{n} A_i * X_i}{A_{catchment}} \tag{4}$$

Where n is the number of grid cells within the catchment, X_i is the value of the variable in cell i, and A_i is the fraction of the grid cell area within the catchment.

Annual maxima were then identified for all variables. For precipitation, two variables were analysed: the annual maximum of daily precipitation (Eq. 5) and the annual maximum of PP7_{daily} (Eq. 6). For temperature, the variable of interest was the annual maximum of daily values (Eq. 7).

$$PP_{\text{max}_{\text{annual}}} = \max(PP_{\text{daily}}) \tag{5}$$

$$PP7_{max_{annual}} = \max(PP7_{daily}) \tag{6}$$

$$Z30 \quad T_{\text{max}_{\text{annual}}} = \max(T_{\text{daily}}) \tag{7}$$

For soil moisture, three variables were computed: the annual maximum of three hourly values (Eq. 8), the annual maximum of SM3_{daily,i} (Eq. 9), and the annual maximum of SM7_{daily,i} (Eq. 10).

$$235 \quad SM_{\text{max}_{\text{annual}}} = \max(SM_{3h}) \tag{8}$$

$$SM3_{max\,annual} = max(SM3_{daily}) \tag{9}$$

$$SM7_{max_{annual}} = max(SM7_{daily})$$
 (10)

All variables were calculated for the period 2000-2021 and for each of the 38 catchments, yielding 7 time series per catchment.

These were further grouped into the nine climatic zones summarised in Table 1.

Regarding streamflow, the variable of interest was maximum hourly discharge (Eq. 11). Streamflow records were collected and used from 38 gauging stations, which contained gaps due to both natural and operational factors. Because the analysis relies on annual maxima, it was essential to reconstruct missing data to avoid introducing bias. To achieve this, a log-linear regression approach (Eq. 12) was applied, using nearby stations within the same study zone as donor sites. For each gap, the donor station was selected based on the best fit during overlapping periods, ensuring consistency and reliability in the reconstructed time series.





$$Q_{max_{annual}} = \max(Q_{hourly}), \qquad (11)$$

$$\ln(Q_{objective}) = b_0 + b_1 \ln(Q_{donor}), \tag{12}$$

Where $Q_{objective}$ is the discharge at the station with missing data, Q_{donor} is the discharge at the donor station, and b_0 and b_1 are regression coefficients. The performance of each infilled record was assessed using three statistics: the coefficient of determination (R^2), the Nash–Sutcliffe Efficiency (NSE), and the Percentage of Bias (PBIAS).

255 **2.3.2** Trend detection

260

270

275

To evaluate temporal changes in the variables, two non-parametric tests were applied: the Mann–Kendall (MK) trend test (Mann, 1945; Kendall, 1975) and the Theil–Sen slope estimator (Theil, 1950; Sen, 1968). The MK test is widely recommended for climatological and hydrological analyses because it does not require data to follow a specific distribution and is effective at detecting monotonic trends. It provides two main outputs: the standardised test statistic (Z) and its associated significance level (p-value). A positive Z indicates an increasing trend, while a negative Z indicates a decreasing trend. The null hypothesis assumes no significant trend, and it is rejected when v-p < 0.1. The Theil–Sen slope estimator complements this analysis by quantifying the trend's magnitude as the median slope across all pairwise data points, providing a robust, unbiased measure of the rate of change over time.

2.4 Correlation analysis

To examine the relationships among the hydrological and meteorological variables, a correlation analysis was performed using the Spearman rank correlation coefficient (Eq. 13). This non-parametric test is suitable for identifying monotonic relationships between variables, as it does not assume linearity or normality in the data distribution (Spearman, 1904). It is therefore widely used in hydrology and climatology to assess associations between climatic drivers and hydrological responses (Gudmundsson et al., 2011; Giuntoli et al., 2013; Zhang et al., 2012).

$$\rho = 1 - \frac{6 \cdot \sum d_i^2}{n \cdot (n^2 - 1)} \tag{13}$$

Where n denotes the number of data points and d_i represents the difference between the ranks of paired observations. The rank of each observation corresponds to its relative position in the ordered dataset. Values of ρ range from -1 (perfect negative correlation) to +1 (perfect positive correlation), with values near 0 indicating weak or no association.



280

285

295



In this study, the Spearman test was applied to all possible pairwise combinations of the seven annual maximum variables across the 38 catchments. This approach allowed us to identify the degree of association between streamflow extremes and potential drivers, including precipitation, temperature, and soil moisture, as well as their short-term accumulation and averaging indices. By comparing correlation structures across climatic zones, we evaluated how the dominant hydro-climatic controls vary spatially. The rationale for using Spearman correlation is that hydrological processes often display non-linear and heterogeneous responses to climatic forcing, particularly in regions such as Chile, where climate gradients are sharp and hydrological regimes are diverse. For instance, previous studies have shown that extreme streamflow events are more strongly linked to precipitation accumulation than to single-day rainfall in Mediterranean climates (Mediero et al., 2014; Blöschl et al., 2019), while soil moisture has been identified as a key mediator between precipitation and runoff in humid and temperate catchments (Wasko & Nathan, 2019; Berghuijs et al., 2019). Conversely, in snow-dominated or arid regions, temperature and snowmelt dynamics often exert stronger control on streamflow variability (Viviroli et al., 2011; Zhai & Tao, 2017). Accordingly, this methodological framework not only quantifies pairwise relationships but also provides the basis for interpreting regional differences in the results section.

290 3 Results

This section presents the main findings of the study regarding the temporal evolution of streamflow regimes and their relationships with meteorological drivers and soil moisture across 38 catchments in Chile. Results are structured as follows: first, streamflow trends; then, precipitation and temperature extremes; and finally, soil moisture dynamics. Finally, the correlation analysis integrates these variables to assess the strength and direction of their associations across contrasting climatic zones. The outcomes are reported at both the catchment and climatic-zone scales, highlighting both consistent patterns and regional differences. Together, these results provide a basis for identifying the dominant hydroclimatic controls on streamflow variability across diverse climatic conditions.

3.1 Trend analysis

3.1.1 Streamflow trends

The analysis of annual maximum streamflow for the period from 2000 to 2021 shows predominantly negative trends across the study catchments (Fig. 2), particularly in the mediterranean (Csb and ET(s)–Csb(h)–Csc) and temperate (Cfb(i)–Cfb) climatic zones, where significant and large-magnitude declines prevail (Fig. 2). Within the Csb zone, decreases are concentrated in the central and western sectors of the study area, which are almost entirely dominated by warm summer mediterranean climates with winter rainfall. In the ET(s)–Csb(h)–Csc zone, the steepest declines occur in catchments influenced by high-altitude warm-summer and cold-summer mediterranean climates, with a secondary contribution from





tundra areas. The shared presence of mediterranean regimes suggests that these regions are susceptible to reductions in precipitation, with higher elevation modulating the magnitude of these declines.

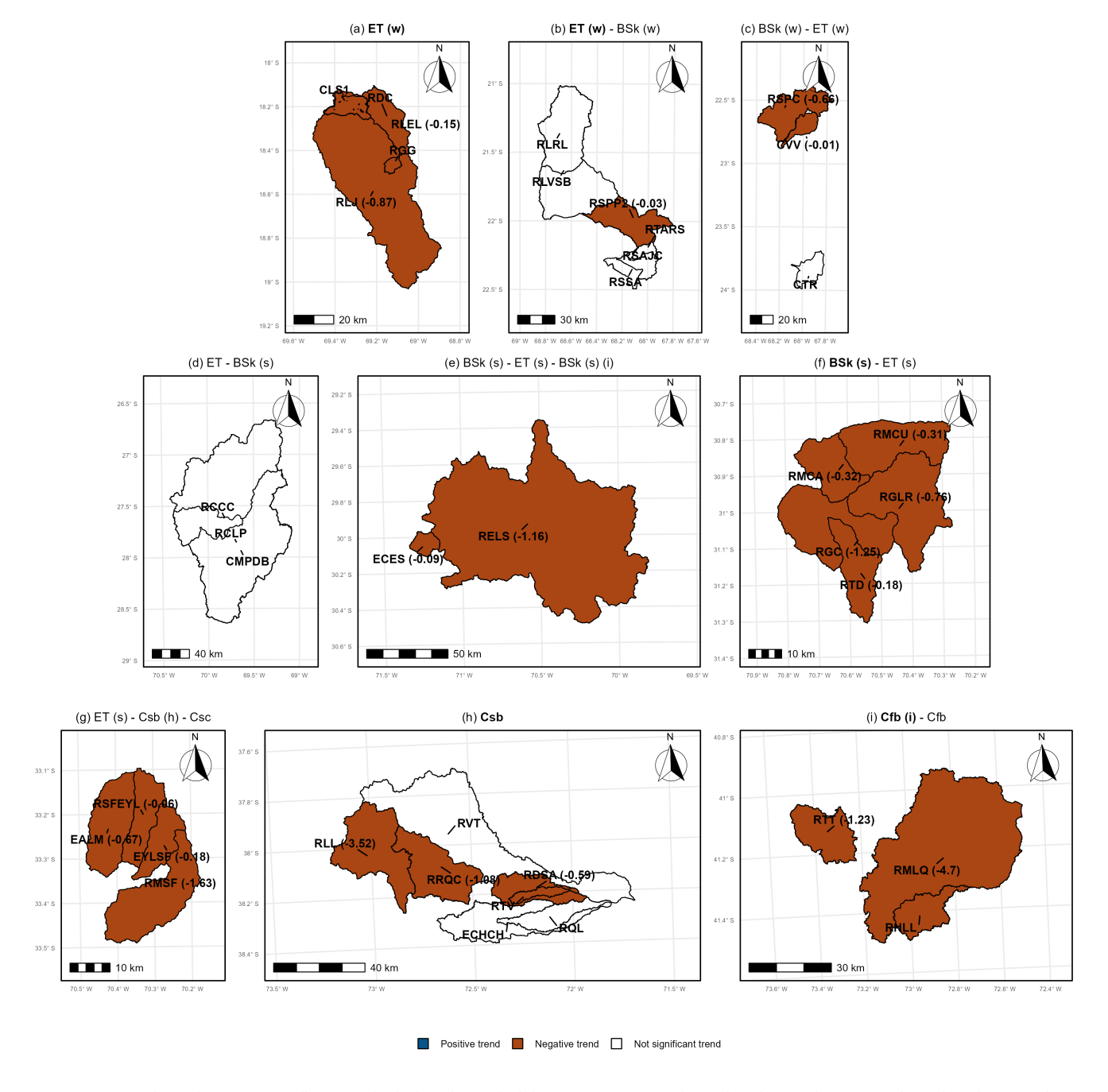


Figure 2. Annual maximum streamflow trends during the period from 2000 to 2021 from the nine study zones. The values in parentheses next to the catchment names represent the Theil–Sen slope values.

https://doi.org/10.5194/egusphere-2025-5318 Preprint. Discussion started: 12 November 2025

© Author(s) 2025. CC BY 4.0 License.



315

320



In temperate rainy zones (Cfb(i)–Cfb), significant negative trends are also evident, especially in the largest catchments. For example, the RMLQ catchment exhibits one of the steepest declines, underscoring the marked reduction in streamflow extremes in temperate coastal-influenced climates, though this effect extends partially inland. Overall, regions characterised by intense winter rainfall display the most consistent downward signals in streamflow maxima.

In semi-arid transition zones (BSk(s)–ET(s) and BSk(s)–ET(s)–BSk(s)(i)), negative slopes are also observed but tend to be more heterogeneous and less frequently significant, likely reflecting oceanic influence and differences in catchment size. In the BSk(s)–ET(s) zone, more substantial declines occur in the Río Grande catchments, where the cold semi-arid climate with winter rainfall predominates. At the same time, weaker signals are detected further south, where the influence of the tundra slightly increases. In the BSk(s)–ET(s)–BSk(s)(i) zone, the RELS catchment shows a much steeper decrease than the ECES catchment, highlighting the regulatory effect of coastal influences on streamflow variability.

In the ET-BSk(s) zone, no significant trends were detected due to the strong regulation by the Lautaro Reservoir, which masks natural streamflow variability. In the northern study area (BSk(w)–ET(w)), only slight downward trends were found, likely linked to localised summer rainfall events. Similarly, in the ET(w)–BSk(w) zone, trends were dispersed and mostly non-significant, with both weak negative and occasional positive slopes, suggesting the influence of localised extreme summer events rather than consistent climate-driven signals.

In tundra-dominated zones (ET(w)), significant declines appear mainly in larger catchments, where decreases intensify with catchment size. This pattern suggests that reduced snowmelt contributions are the dominant factor, given that these summerrainfall regions are primarily influenced by tundra climates, with minimal contributions from semi-arid zones.

In summary, the most robust signal is the consistent decline in maximum streamflow in mediterranean and temperate climates, followed by other winter-rainfall climates and, to a lesser extent, tundra climates. These patterns align with broader hydroclimatic drivers, namely reduced precipitation and increasing temperatures across central and southern Chile (Oertel et al. 2020; Salazar et al. 2024).

3.1.2 Precipitation and temperature trends

Annual maximum precipitation shows a predominantly negative signal across the study area, with the strongest and most consistent decreases in the mediterranean (Csb and ET(s)–Csb(h)–Csc) and temperate (Cfb(i)–Cfb) zones (Fig. 3). In the Csb zone, significant declines are concentrated in the western catchments, coinciding with the areas that also displayed marked streamflow reductions. In the ET(s)–Csb(h)–Csc zone, all catchments exhibited significant and large-magnitude declines,





making this the most affected climatic setting. These patterns are consistent with the influence of winter-rainfall mediterranean climates. They are further modulated by elevation, which reduces the frequency of intense frontal systems and is associated with the upward shift of the 0 °C isotherm.

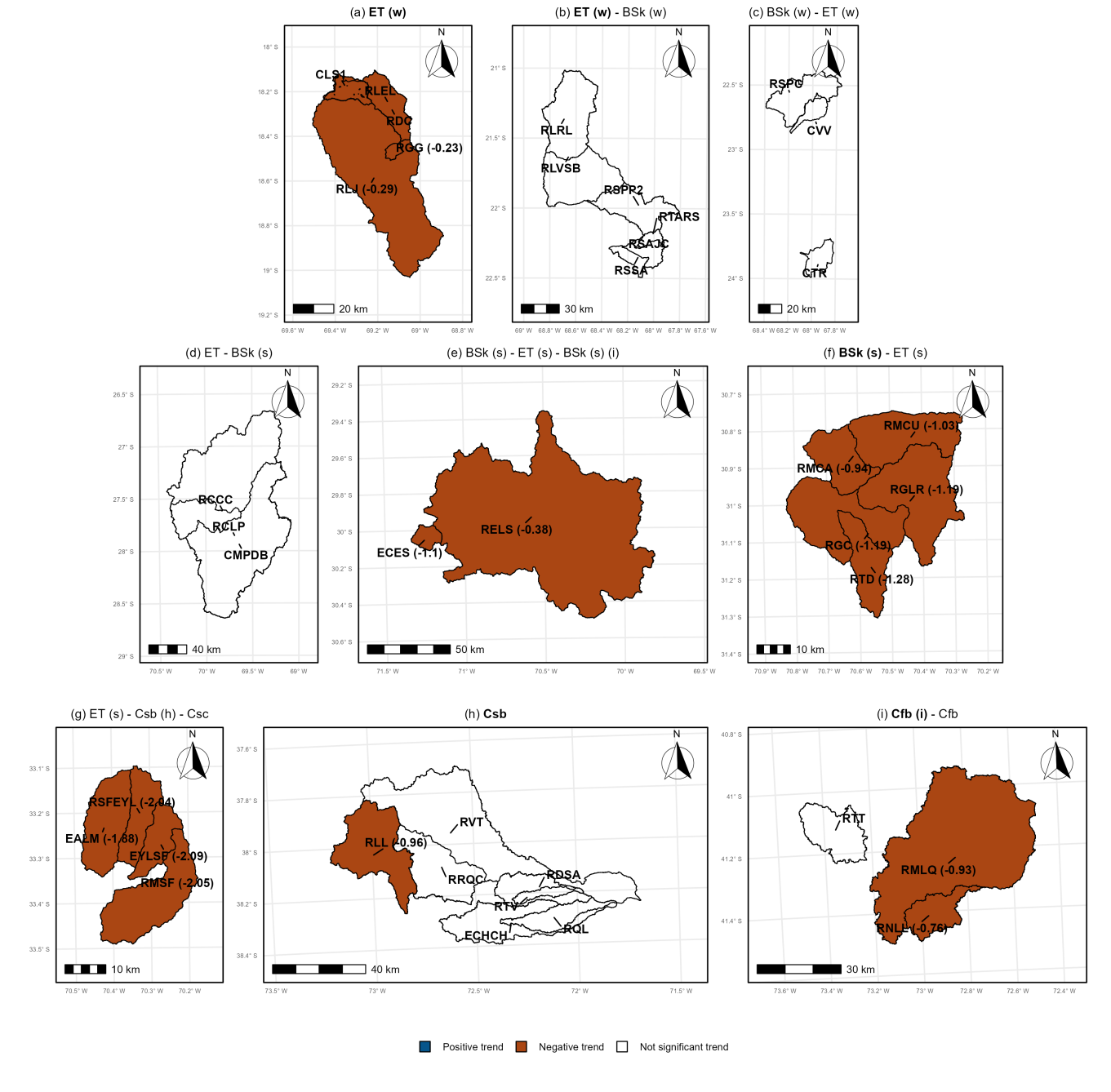


Figure 3. Annual maximum precipitation trends during the period from 2000 to 2021 in the nine study zones. The values in parentheses next to the catchment names represent the Theil–Sen slope values.





In semi-arid winter-rainfall zones (BSk(s)–ET(s)), significant negative trends were also detected, reinforcing the regional pattern of precipitation decline across winter-rainfall climates. In the BSk(s)–ET(s)–BSk(s)(i) zone, negative slopes were present but generally weaker and less frequently significant. For example, the RELS – strongly influenced by a tundra climate with winter rainfall – showed only mild decreases. In contrast, the ECES catchment, dominated by cold semi-arid winter rainfall and coastal influence, exhibited stronger negative slopes. In tundra and summer-rainfall influenced zones (ET(w)–BSk(w), ET–BSk(s), and BSk(w)–ET(w)), precipitation trends were weaker, more heterogeneous, and mostly non-significant, highlighting the dominant role of snowmelt or summer convective rainfall in these regions. In the temperate rainy zone (Cfb(i)–Cfb), significant negative slopes were found, particularly in coastal-influenced catchments such as Río Maullín, reinforcing the evidence of sustained precipitation declines in oceanic climates.

Seven-day accumulated precipitation provided an even stronger and more consistent signal of decline (Fig. 4). In the Csb zone, a larger number of catchments displayed significant decreases, with only those in the southeast remaining non-significant. In the ET(s)–Csb(h)–Csc zone, all catchments showed reinforced negative slopes, confirming this as the climatic zone with the most pronounced reduction in multi-day rainfall events. In temperate rainy zones, the catchment closest to the coast also shifted from non-significant to significant, indicating that prolonged rainfall extremes are declining even in ocean-moderated regions. In semi-arid zones, the magnitude of decreases in seven-day precipitation was generally greater than for single-day maxima.

By contrast, in tundra and summer-rainfall regions, signals remained weak and mostly non-significant, reaffirming the limited role of rainfall extremes in snowmelt-dominated zones. These findings indicate that precipitation reductions affect not only isolated daily extremes but also longer-duration events, which are critical for runoff generation.

Temperature extremes exhibit a contrasting signal, with a consistent, though modest, warming trend across nearly all climate zones (Fig. 5). In Mediterranean and temperate winter-rainfall regions, upward trends were statistically significant in several catchments, reflecting both regional warming and the elevation-driven upward shift of the 0 °C isotherm. In coastal temperate catchments, the most significant increases were observed, indicating that ocean warming is now influencing a climate zone traditionally stabilised by maritime conditions. In semi-arid zones, warming trends were generally positive and more pronounced in drier basins. In contrast, trends in tundra and summer-rainfall regions were weaker and mostly non-significant due to the high variability of summer events.





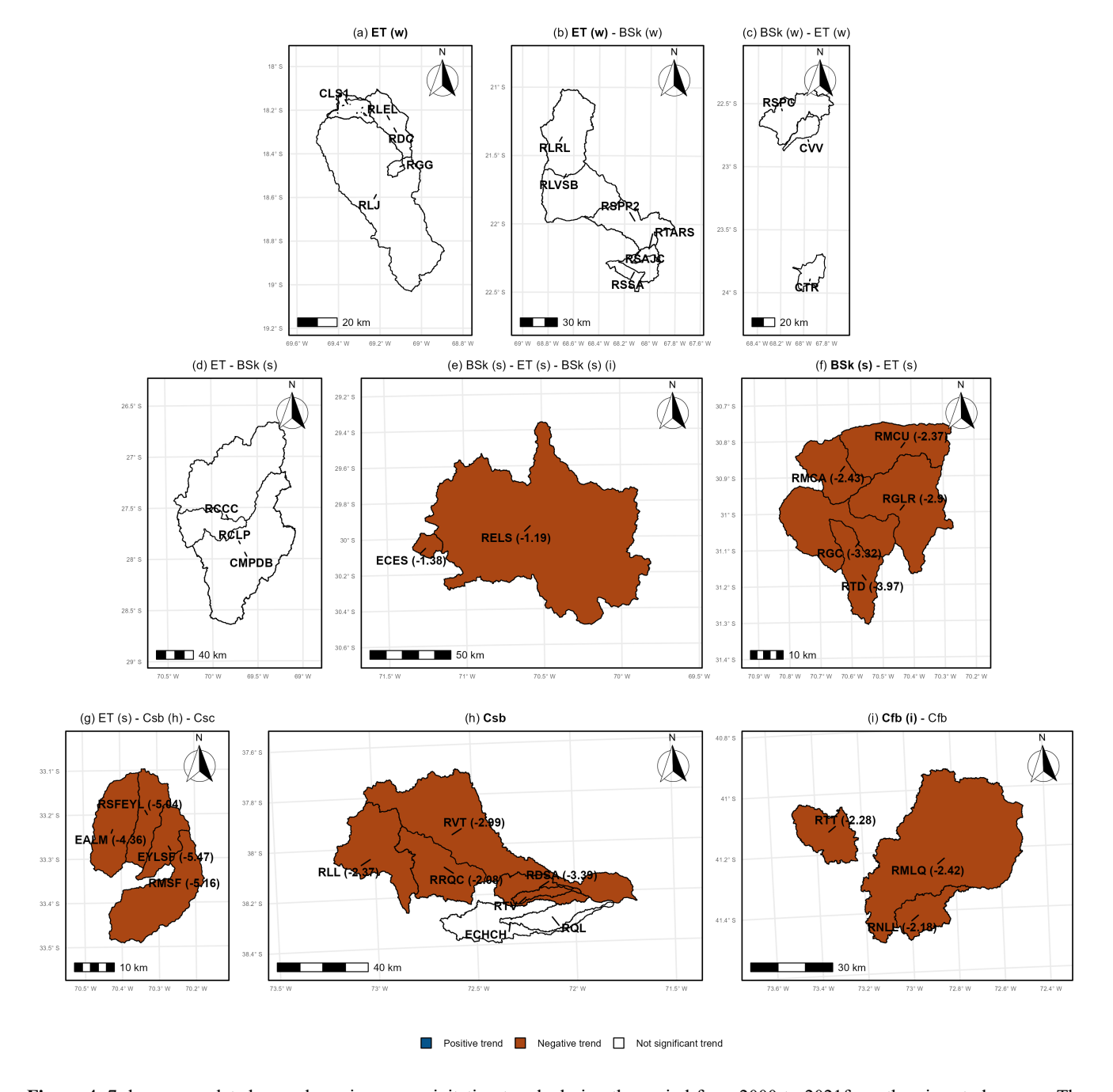


Figure 4. 7-day accumulated annual maximum precipitation trends during the period from 2000 to 2021 from the nine study zones. The values in parentheses next to the catchment names represent the Theil–Sen slope values.

Overall, the results reveal a consistent hydro-climatic signal: precipitation extremes – both daily and accumulated – are declining in mediterranean, temperate, and semi-arid winter-rainfall regions, while temperature maxima are increasing across





the entire study area. This dual pattern of decreasing rainfall and rising temperatures provides a coherent explanation for the robust declines in streamflow identified in central and southern Chile.

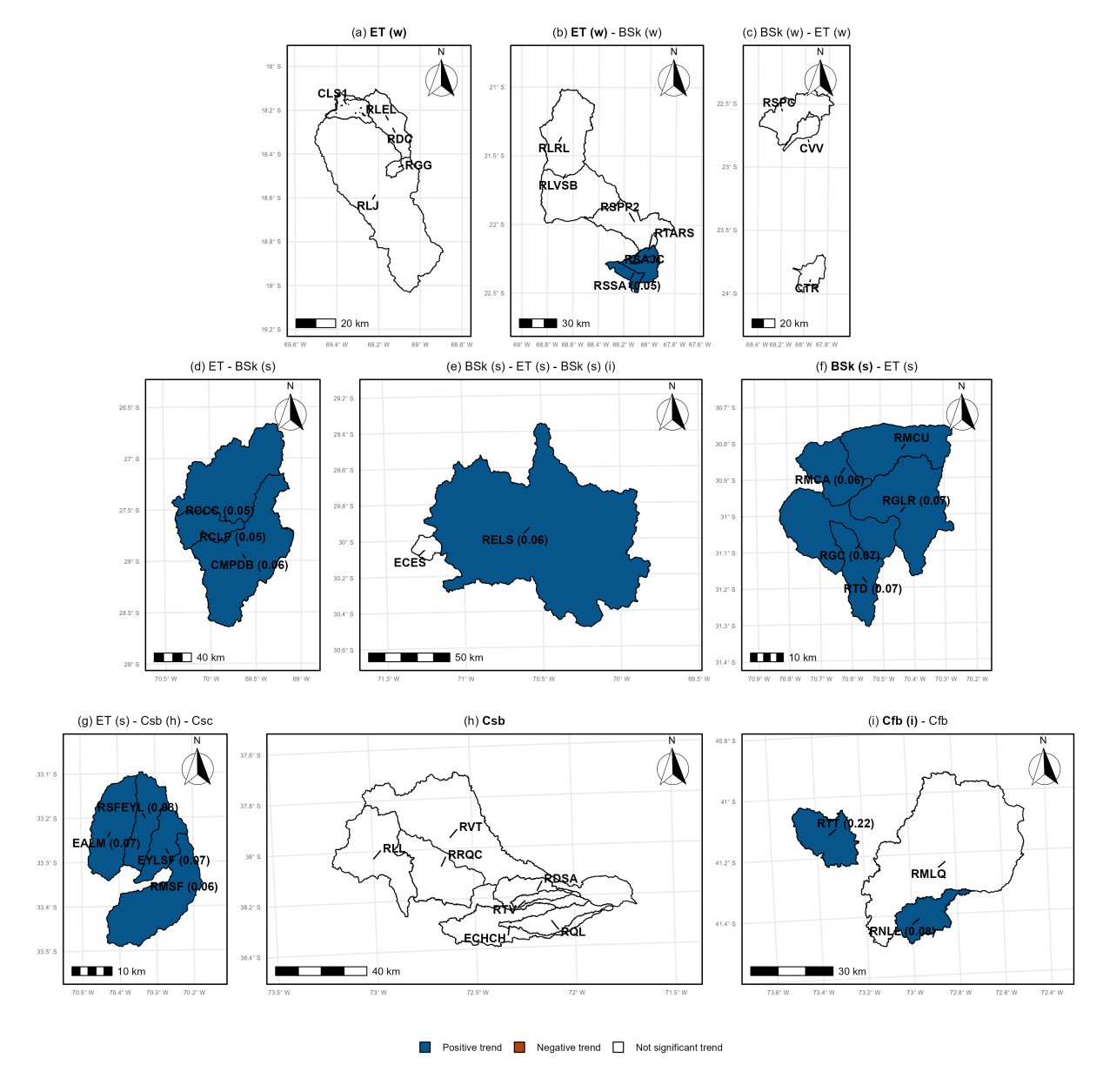


Figure 5. Annual maximum temperature trends during the period from 2000 to 2021 in the nine study zones. The values in parentheses next to the catchment names represent the Theil–Sen slope values.



390

395

410

415



3.1.3 Soil moisture trends

Annual maximum soil moisture trends (Fig. 6) are generally downward, although they are not as pronounced as those observed for streamflow and precipitation. Nonetheless, the drying signal is more evident than the warming detected in temperature extremes. In cold semi-arid climates with winter rainfall, all catchments showing significant results presented decreasing soil moisture. In the BSk(s)–ET(s) zone, this was concentrated in the northwestern sector, while in the BSk(s)–ET(s)–BSk(s)(i) zone, both catchments displayed negative trends regardless of coastal influence. By contrast, in arid zones influenced by summer rainfall (ET(w)–BSk(w) and BSk(w)–BWk(w)), significant positive trends emerged. In the ET(w)–ET(w) zone, increases were observed in the northern sector, which is dominated by tundra influence, while in the BSk(w)–ET(w) zone, they occurred in the south, where cold semi-arid conditions prevail. These results suggest that in drier summer-rainfall regions, irregular rainfall events may counterbalance drying tendencies when soil moisture is measured at a three-hour resolution.

In the ET-BSk(s) zone, no significant trends were detected, making this one of the least affected areas in terms of soil moisture change. In the ET(w) zone, significant downward trends were observed in the north; however, these were attributed to reservoir regulation, suggesting a localised rather than regional effect. Overall, tundra climates with summer rainfall did not display consistent significant changes, but rather a regional effect. In temperate rainy climates (Cfb(i)–Cfb), negative soil moisture trends were also present, albeit weaker than in arid winter-rainfall regions. These decreases are consistent with precipitation declines, highlighting a drying tendency even in traditionally humid environments. In the Csb zone, catchments in the north exhibited mild downward slopes, while in the ET(s)–Csb(h)–Csc, results were non-significant, indicating that high-altitude mediterranean regions – naturally characterised by lower soil water content – are less sensitive to soil moisture extremes.

Three-day averaged soil moisture (Fig. 7) revealed that previously significant trends in the BSk(s)–ET(s) disappeared, but declines persisted in the BSk(s)–ET(s)–BSk(s)(i) zone, suggesting that coastal influence and tundra contributions amplify drying signals in semi-arid regions. In the ET(w)–BSk(w), upward trends in the north remained, though less pronounced. In the Cfb(i)–Cfb, significant decreases persisted, but smoothing attenuated their magnitude. In the Csb zone, all catchments exhibited negative slopes, albeit weaker than those in the three-hourly datasets, suggesting an overall reduction in soil moisture. In the ET(s)–Csb(h)–Csc, no significant results were detected. By contrast, in the ET(w) zone, significant downward trends were observed across the entire study area, with the most substantial decreases occurring in the north, indicating progressive soil drying driven by reduced rainfall and snowmelt.





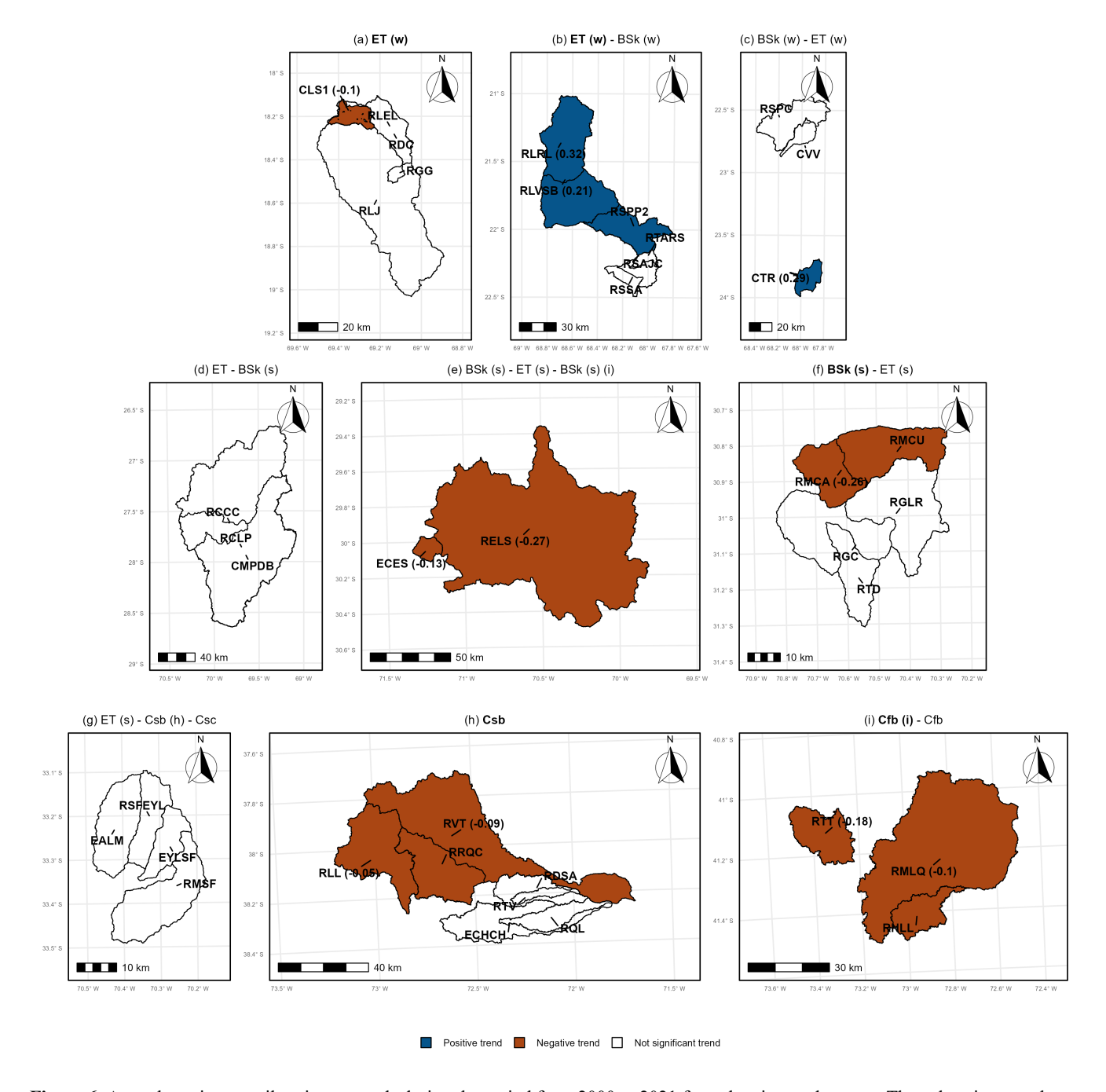


Figure 6. Annual maximum soil moisture trends during the period from 2000 to 2021 from the nine study zones. The values in parentheses next to the catchment names represent the Theil–Sen slope values.





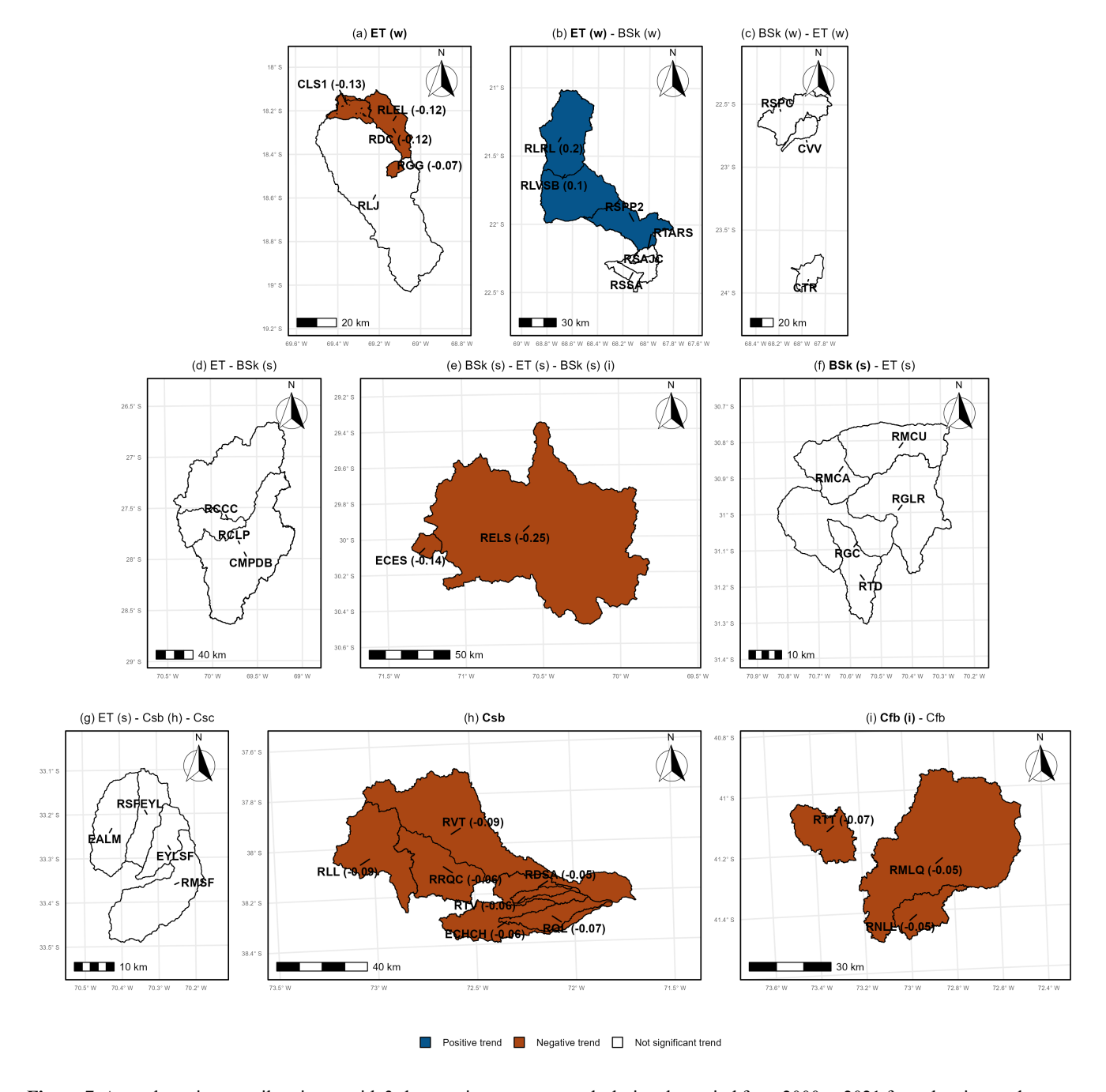


Figure 7. Annual maximum soil moisture with 3-day moving average trends during the period from 2000 to 2021 from the nine study zones. The values in parentheses next to the catchment names represent the Theil–Sen slope values.





The seven-day-averaged soil moisture (Fig. 8) confirmed the results from the three-day average, reinforcing the general patterns across the climate zones. The smoothing effect enabled more precise identification of regional tendencies, confirming drying in mediterranean and temperate climates, as well as semi-arid regions with tundra contributions. In contrast, summerrainfall-dominated zones showed more heterogeneous or upward trends.

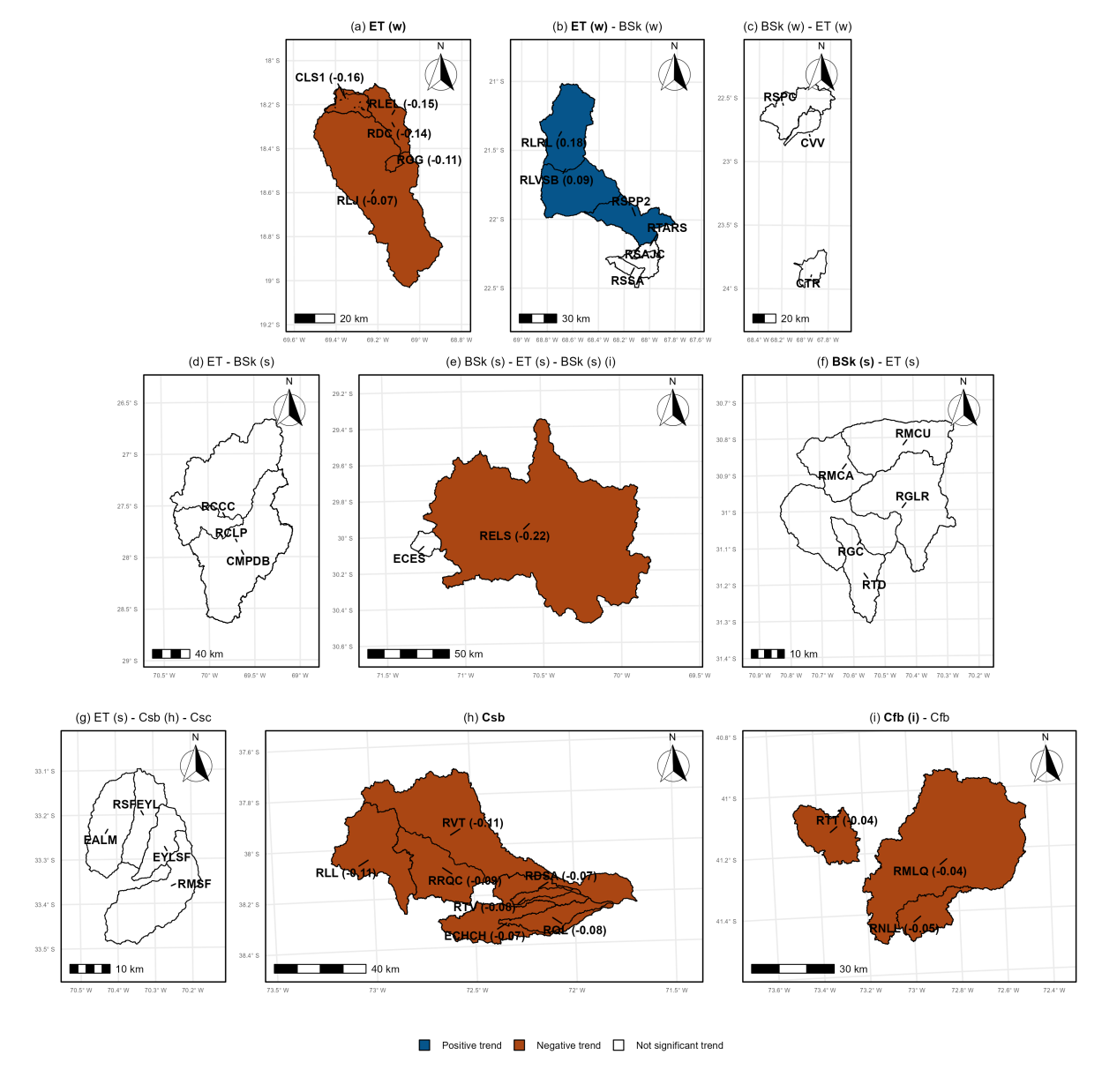


Figure 8. Annual maximum soil moisture with 7-day moving average trends during the period from 2000 to 2021 from the nine study zones. The values in parentheses next to the catchment names represent the Theil–Sen slope values.



445

450

455



Overall, soil moisture extremes are declining across most winter-rainfall climates, particularly in semi-arid and temperate regions, where precipitation reductions and temperature increases are acting in tandem. In summer-rainfall climates, however, the signal is weaker or even positive, reflecting the irregular nature of precipitation events during that season.

To provide an integrated view of the hydroclimatic tendencies identified across the study area, Table 2 summarises the direction and significance of trends for all variables and climatic zones. Southern catchments, which are dominated by mediterranean and temperate winter-rainfall regimes, exhibit a higher proportion of significant negative trends in maximum precipitation (both daily and seven-day accumulations), streamflow, and soil moisture. By contrast, northern catchments, characterised by semi-arid and tundra summer-rainfall climates, show more heterogeneous or positive soil-moisture trends and fewer significant changes in precipitation and streamflow. This contrast highlights the dominant role of precipitation variability in shaping hydrological responses in winter-rainfall regions, whereas in northern zones, snowmelt and irregular summer rainfall buffer or counterbalance drying signals. The positive or neutral soil-moisture responses observed in these northern zones align with the absence of consistent precipitation trends. In contrast, in the south, synchronous declines in precipitation, streamflow, and soil moisture reflect a broader drying tendency driven by climatic forcing. Overall, the results indicate a pronounced drying tendency in central and southern Chile, where winter-rainfall climates prevail, highlighting the combined effects of reduced precipitation inputs and increasing temperatures on streamflow generation.

Table 2. Summary of trend directions and significance across climatic zones. Positive trends are shown in blue, negative trends in red, and non-significant trends are uncoloured.

Zone	Number of stations	Q trend	PP trend	PP7 trend	T trend	SM trend	SM3 trend	SM7 trend
ET (w)	5	2/3	2/3	5	5	1/4	4/1	5/0
ET (w) - BSk (w)	6	1/5	6	6	1/5	2/4	2/4	2/4
BSk (w) - ET (w)	3	2/1	3	3	3	1/2	3	3
ET - BSk (s)	3	3	3	3	3/0	3	3	3
BSk (s) - ET (s) - BSk (s) (i)	2	2/0	2/0	2/0	1/1	2/0	2/0	1/1
BSk (s) - ET (s)	5	5/0	5/0	5/0	4/1	1/4	5	5
ET (s) - Csb (h) - Csc	4	4/0	4/0	4/0	4/0	4	4	4
Csb	7	3/4	1/6	4/3	7	2/5	7/0	7/0
Cfb (i) - Cfb	3	2/1	2/1	3/0	2/1	2/1	3/0	3/0

The hydro-climatic patterns identified in the mediterranean and temperate zones of Chile mirror those observed in other winterrainfall regions worldwide. In Southern Europe, widespread streamflow declines linked to warmer and drier conditions have been reported in Spain (Yeste et al., 2018), central Italy (Gentilucci and Hamed, 2023), and Cyprus (Myronidis et al., 2018), confirming the high sensitivity of mediterranean hydroclimates to concurrent decreases in precipitation and rising temperatures. Similar signals have been found in semi-arid regions, where enhanced evapotranspiration offsets rainfall gains, https://doi.org/10.5194/egusphere-2025-5318 Preprint. Discussion started: 12 November 2025

© Author(s) 2025. CC BY 4.0 License.



EGUsphere Preprint repository

as documented in northeastern Iran (Minaei and Irannezhad, 2018) and in arid and warm-dry areas of North America and Australia (Do et al., 2017). In contrast, high-elevation and snow-dominated systems show weak or mixed trends, consistent with observations from the Hindu Kush–Karakoram–Himalaya (Hasson et al., 2017) and northern China (Xu et al., 2024; Lu et al., 2025), where temperature exerts stronger control on runoff generation than precipitation. Overall, these international comparisons reinforce that the drying tendencies identified in central and southern Chile (Oertel et al., 2020; Sangüesa, 2023; Alvarez-Garretón et al., 2021) are part of a broader global pattern affecting winter-rainfall climates, as also emphasised by the IPCC (2023).

3.2 Correlation analysis

The correlation analysis provides insight into the relationships among streamflow, precipitation, temperature, and soil moisture across the study catchments. Overall, the results confirm the central role of precipitation – particularly seven-day accumulated precipitation – in explaining both streamflow and soil moisture variability. At the same time, temperature plays a more decisive role in tundra and arid climates. Soil moisture emerges as an intermediate variable, strongly associated with precipitation, and in mediterranean and temperate climates, it modulates runoff responses.

Across all climate zones, strong positive correlations are consistently observed between precipitation and accumulated precipitation, as well as among the different soil moisture variants. Streamflow exhibits strong positive correlations with accumulated precipitation, underscoring the importance of multi-day rainfall events for runoff generation in winter-rainfall climates. To illustrate representative cases, we retain in the main text the correlation matrices for the mediterranean zone (Fig. 9), the semi-arid winter zone (Fig. 10), and the tundra summer zone (Fig. 11), as these capture the dominant patterns across contrasting hydro-climatic regimes. The remaining figures for the other climatic areas are provided as Supplementary Material S2 for reference.

Streamflow-soil moisture relationships are generally weaker but strengthen when smoothed indices (3- and 7-day averages) are used, reflecting the buffering role of soil storage. This effect is evident in mediterranean and temperate coastal zones. In these climates, precipitation and soil moisture jointly control streamflow responses, confirming that soil water retention reduces direct runoff from rainfall events. Temperature correlations are weaker and less consistent. In mediterranean and temperate zones, its influence on precipitation, soil moisture, and streamflow is minimal. However, in tundra and semi-arid zones, temperature exhibits stronger negative correlations with both streamflow and soil moisture, especially when soil moisture is smoothed. This indicates that rising temperatures exacerbate drying processes by enhancing evapotranspiration and reducing snowmelt contributions.

490

485

470





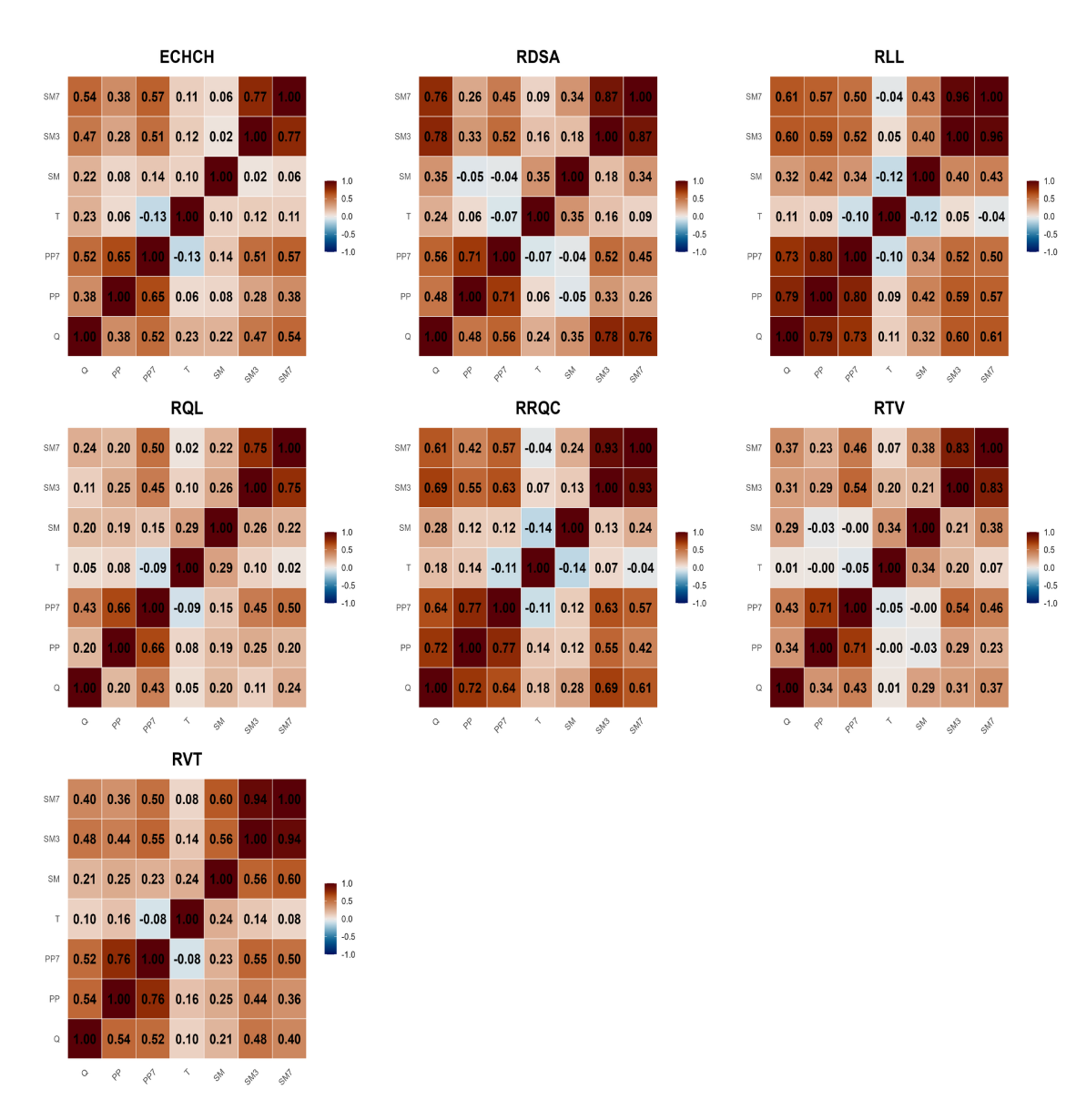


Figure 9. "Csb" correlation matrices for all combinations of variables.





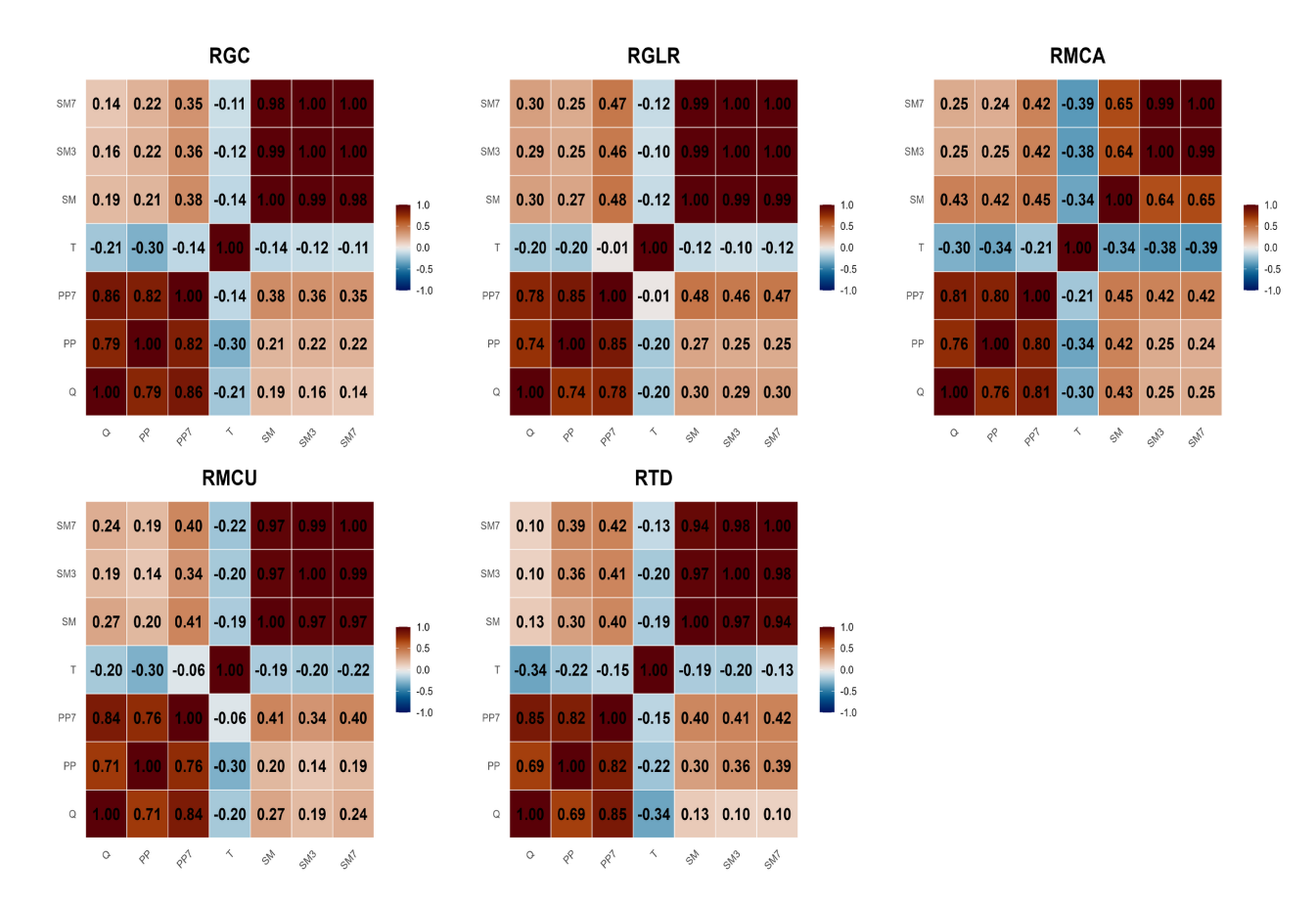


Figure 10. "BSk (s) - ET (s)" correlation matrices for all combinations of variables.



505

510



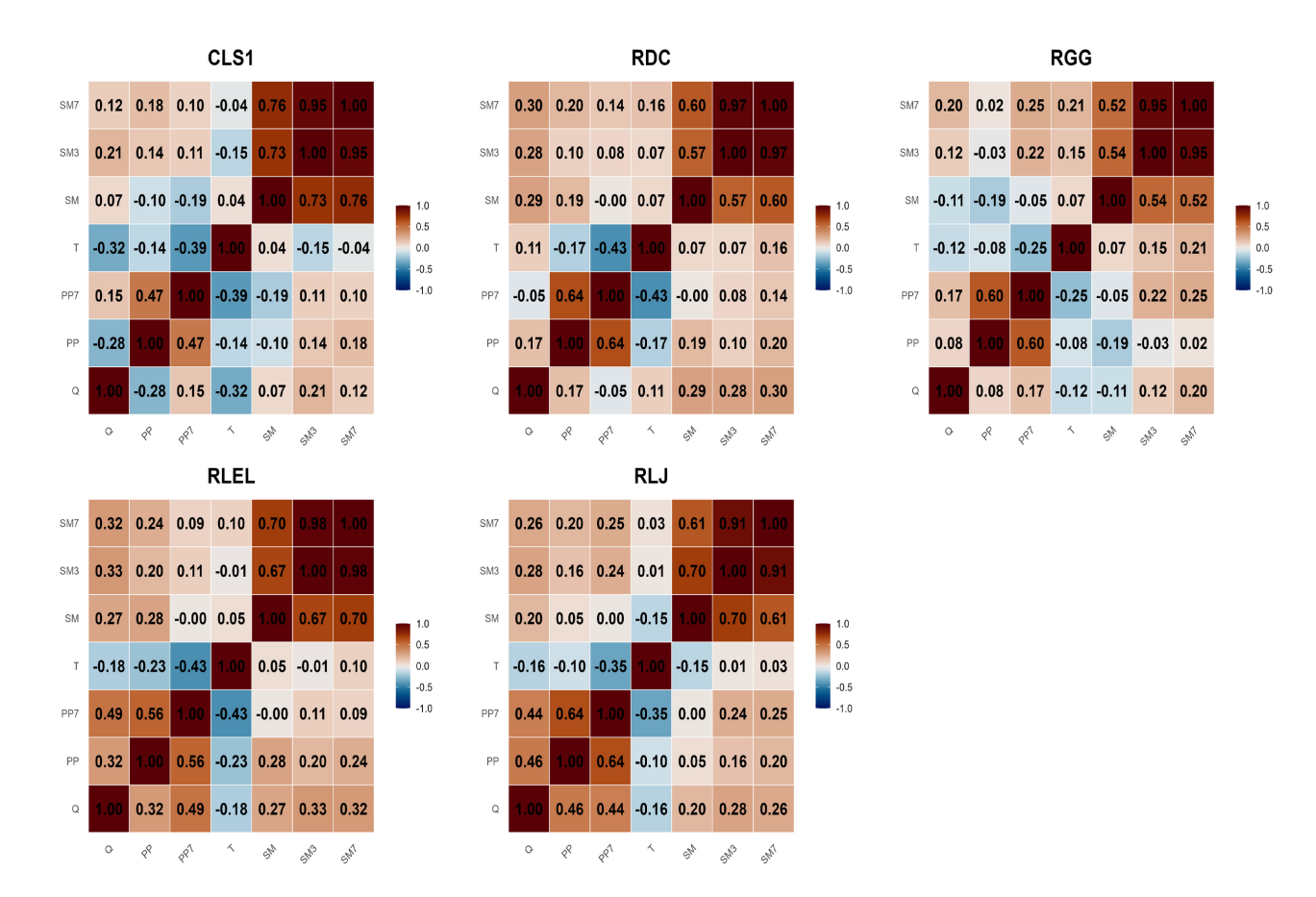


Figure 11. "ET (w)" correlation matrices for all combinations of variables.

At the climate-zone scale, three main patterns emerge: 1) Winter-rainfall regions (mediterranean, temperate, semi-arid): Streamflow is strongly correlated with precipitation, especially with accumulated values. Soil moisture reinforces this relationship when smoothed. 2) Summer-rainfall and tundra regions: Correlations are weaker and more heterogeneous. Precipitation plays a less decisive role, while temperature exerts stronger control on soil moisture and streamflow. 3) Regulated watersheds: In watersheds affected by reservoirs (e.g., Lautaro), natural hydro-climatic controls are masked, and correlations do not represent natural streamflow responses.

Across climatic zones, the synthetic heatmap (Fig. 12) provides a concise overview of the median correlations among hydrometeorological variables. Results consistently confirm strong positive relationships between streamflow and precipitation, particularly when considering seven-day accumulated precipitation (PP7), highlighting the central role of multi-day rainfall events in runoff generation under winter-rainfall climates. Precipitation–soil moisture correlations (PP–SM3 and PP7–SM3) are also positive and stronger for accumulated values, indicating that soil water recharge depends more on sustained



520



precipitation than on isolated extremes. Streamflow–soil moisture relationships (Q–SM3) are positive but weaker, reflecting the buffering role of antecedent soil moisture in modulating runoff response. Conversely, temperature exhibits predominantly negative correlations with both streamflow (T–Q) and soil moisture (T–SM3), with stronger magnitudes in tundra and summerarid climates. This pattern suggests that warming amplifies evapotranspiration and reduces snow contributions, ultimately limiting water availability. Together, these results emphasise three key aspects: (i) the dominance of accumulated precipitation in driving streamflow extremes, (ii) the role of soil moisture as an intermediate control between precipitation and runoff, and (iii) the increasing adverse effect of temperature in climates where snowmelt and soil water storage are crucial for sustaining discharge.

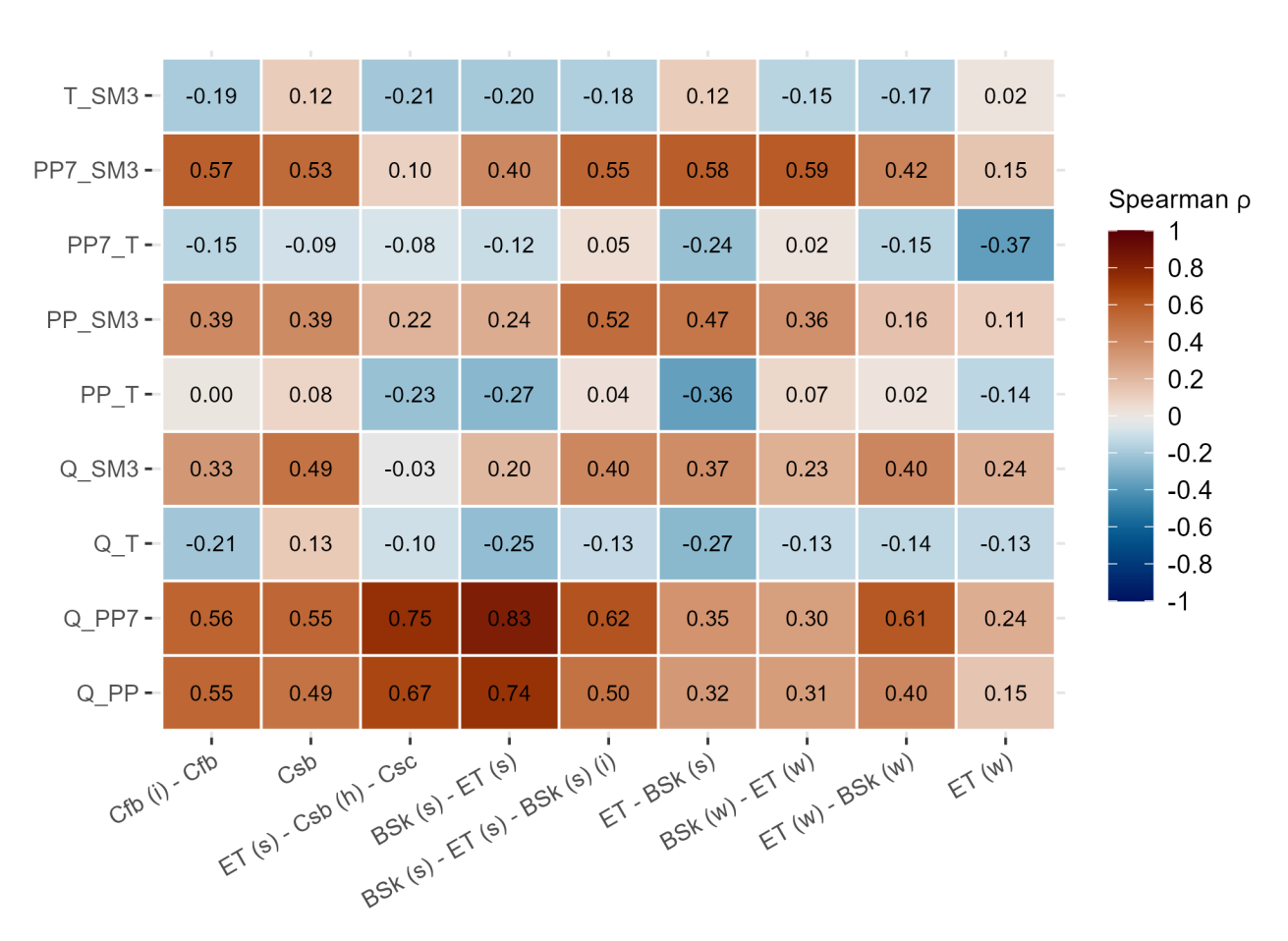


Figure 12. Synthetic heatmap of average correlations across climatic zones.





4 Discussion

4.1 Trends

535

545

550

The streamflow trends reveal a clear and consistent decrease across Mediterranean, temperate, and winter-rainfall climates, indicating a strong sensitivity to winter precipitation, as also observed in Europe (Blöschl et al., 2019). These declines are likely driven by reduced winter rainfall and enhanced evapotranspiration under warmer conditions, linked to the megadrought and the broader global pattern affecting winter-rainfall regions (IPCC 2023). Semi-arid areas exhibit a more heterogeneous but predominantly negative behaviour, consistent with observations in arid and warm-dry regions of North America and Australia (Do et al., 2017) and in northeastern Iran (Minaei and Irannezhad, 2018). This contrast between semi-arid winter-rainfall and summer-rainfall climates highlights that streamflow dependence on precipitation is stronger in the former. In contrast, local and coastal influences modulate or attenuate trends in the latter.

Precipitation also shows mainly negative trends, particularly in mediterranean and temperate zones, which become more evident when considering seven-day accumulated precipitation, including ocean-moderated regions. Similar declines have been reported for central and southern Chile (Oertel et al., 2020; Sangüesa et al., 2023; Stolpe et al., 2016). These findings confirm the critical role of winter precipitation in sustaining streamflow, contrasting with the weaker or non-significant changes found in tundra and summer-rainfall climates.

Global warming intensifies these effects, especially in drier catchments. While Vicuña et al. (2013) proposed that extreme heat might increase the contributing runoff area, the results here indicate that enhanced evapotranspiration instead reduces streamflow availability. Temperature increases across all climates, particularly coastal temperate basins, further reinforce the drying signal.

Soil moisture trends exhibit contrasting behaviour across climatic zones, reflecting the combined influence of precipitation regimes, temperature, and snow dynamics. In winter-rainfall climates – particularly mediterranean, temperate, and semi-arid regions – soil moisture shows predominantly negative or non-significant trends, consistent with the joint effects of declining precipitation and increasing temperature that limit soil recharge and enhance evapotranspiration. The increasingly negative trends from SM to SM3 and SM7 indicate cumulative water deficits and reduced soil recovery between rainfall events, which, in turn, contribute to the observed declines in streamflow. In contrast, summer-rainfall climates display mostly stable or positive soil moisture trends, especially in semi-arid basins where convective summer storms sustain short-term replenishment despite high temperatures. However, in purely tundra climates, soil moisture shows weak or even opposite signals because snow and frozen ground dominate the hydrological response, reducing the role of soil water storage in runoff generation. Coastal temperate basins, influenced by oceanic humidity, exhibit milder declines, confirming that maritime moderation partially offsets the drying signal. Overall, the spatial variability of soil moisture trends reflects the interplay between



560

565

585



555 precipitation seasonality, temperature-driven evapotranspiration, and the relative importance of snowmelt versus soil water as sources of streamflow. This underscores the need to integrate physical variables, not just meteorological ones, to understand mechanisms of hydrological change.

These consistent patterns suggest that the hydro-climatic behaviour observed in Chile can be extended to other regions with comparable climatic settings. Mediterranean and winter-rainfall climates worldwide appear to share a drying trajectory, driven by declining precipitation and rising temperatures, as documented in southern Europe (Yeste et al., 2018; Gentilucci and Hamed, 2023; Myronidis et al., 2018) and parts of Australia and North America (Do et al., 2018). Semi-arid climates exhibit greater spatial heterogeneity, yet the predominance of negative streamflow and soil-moisture trends suggests similar vulnerabilities to warming and increased evapotranspiration. Conversely, tundra and summer-rainfall climates exhibit weaker or mixed signals, confirming that snowmelt-dominated and convective systems respond differently to climate forcing. Recognising these consistent responses across climate types is crucial, as it allows extending hydrological inferences to regions with limited observations and supports the development of climate-specific strategies for assessing and managing water resources under global warming.

4.2 Correlations

Correlations confirm that precipitation – especially multi-day accumulation – is the primary driver of streamflow and soil moisture, reinforcing findings from Europe (Blöschl et al., 2019). These relationships are stronger in winter-rainfall climates, where prolonged rainfall events govern runoff generation. Streamflow in tundra climates, however, correlates more closely with temperature than precipitation, reflecting snowmelt control. Specifically, in mediterranean climate (Csb, Csc), we can see a strong precipitation control (ρ = 0.56 ± 0.19), declining trends in all hydroclimatic variables, and high vulnerability to sustained drought. In the case of temperate oceanic climate (Cfb, Cfc), there is a strong precipitation-streamflow correlation (ρ = 0.55 ± 0.2), moderate declining trends, and soil moisture acts as an important intermediate control. For the Cold semi-arid climate (BSk), a weaker precipitation-streamflow coupling (ρ = 0.49 ± 0.21), high interannual variability, and more pronounced temperature effects are observed. In the tundra climate (ET), we encountered mixed streamflow trends, a strong warming signal (+0.07°C/year), and an increasing importance of glacier and permafrost dynamics. Finally, in summer-rainfall regions, complex patterns reflecting ENSO influences, weaker trends but higher inter-annual variability are encountered.

Analysing the different variables, behaviour temperature generally shows weak and inverse correlations, but exerts a stronger influence in tundra and semi-arid climates. Rising temperatures enhance evapotranspiration, reduce snowmelt contributions, and alter soil moisture patterns, consistent with observations in Spain (Yeste et al., 2018) and Cyprus (Myronidis et al., 2018). Soil moisture—streamflow correlations are more evident when using smoothed soil moisture indices, which better reflect storage capacity. In mediterranean and temperate zones, this relationship is direct, indicating that greater soil retention limits

https://doi.org/10.5194/egusphere-2025-5318 Preprint. Discussion started: 12 November 2025

© Author(s) 2025. CC BY 4.0 License.



590

595

600

605

EGUsphere Preprint repository

the immediate runoff response. In contrast, Wasko and Nathan (2019) found the opposite pattern in Australia, where soil moisture better explains streamflow variability when rainfall dependence is low. Here, only tundra climates showed no significant soil moisture–streamflow link, whereas semi-arid regions did, helping clarify previous uncertainty noted by Sangüesa et al. (2023).

In summary, accumulated precipitation is the dominant control of streamflow extremes in mediterranean, temperate, and winter-rainfall climates. Soil moisture acts as an intermediate regulator between precipitation and runoff, while temperature exerts increasingly adverse effects, as snowmelt and soil storage are vital for sustaining discharge. Altogether, these patterns reveal a coherent drying signal across winter-rainfall regions, driven by declining precipitation and rising temperatures, with implications for water availability and hydrological extremes under ongoing climate change.

These relationships are consistent with hydro-climatic dynamics observed in comparable regions worldwide. In mediterranean and temperate climates, the strong dependence of streamflow on accumulated precipitation reflects the dominance of frontal winter systems, similar to patterns reported for southern Europe and Australia (Blöschl et al., 2019; Wasko and Nathan, 2019). In contrast, the weaker, more temperature-driven relationships in tundra and semi-arid climates mirror those of snow- and heat-controlled basins in Asia and North America, where evapotranspiration and melt processes dominate runoff generation. This suggests that the coupling between precipitation, soil moisture, and streamflow observed in Chile can be extended to analogous climates globally, providing a framework for anticipating hydrological behaviour in data-scarce regions. Although flow regulation – such as in the Lautaro reservoir – can dampen or mask streamflow trends, the underlying climate-driven correlations remain largely preserved, confirming that the dominant hydro-climatic controls are robust across both natural and managed catchments.

In analysing the results, certain limitations were considered. The relatively short analysis period (2000–2021) limits the ability to distinguish long-term climate change signals from multi-decadal variability. However, this is partially mitigated by consistency with longer records (Boisier et al., 2018). Land use and land cover changes, such as forest plantations and urban expansion in Chile (Miranda et al., 2017), were not explicitly accounted for but may influence streamflow independently of climate. The coarse spatial resolution of gridded climate datasets (e.g., CR2MET) and satellite soil moisture products introduces uncertainty, particularly in mountainous areas where orographic effects and steep terrain affect data accuracy (Falvey and Garreaud, 2009; Al-Yaari et al., 2019).

5 Conclusion

Climate change represents a major global challenge, particularly regarding water availability and the intensification of global warming. Understanding how streamflow responds to these changes across different climatic regimes is crucial for assessing



625

630

635

640

645



hydrological vulnerability and future water resources. Chile provides an exceptional natural laboratory for this purpose, given its remarkable climatic diversity and the persistent megadrought that has affected much of the country over the past decade.

This study assessed the hydroclimatic controls on streamflow evolution across 38 Chilean catchments spanning nine climate study areas during 2000–2021. By integrating field observations, gridded climate datasets, and satellite-derived soil moisture data, we quantified trends in streamflow, precipitation, temperature, and soil moisture. We examined their relationships across Chile's climatic gradient. The results reveal clear spatial patterns and highlight the dominant climatic drivers shaping hydrological dynamics in the country.

Winter-rainfall regions—particularly mediterranean and temperate climates—exhibit the most consistent and pronounced streamflow declines, with 67% of catchments showing statistically significant negative trends (p < 0.1) and a median rate of -1.12 mm/year. These reductions in streamflow are accompanied by parallel decreases in precipitation (median slope: -1.53 mm/year) and soil moisture (median slope: -0.11 mm/year), indicating a coherent drying signal consistent with the hydroclimatic impacts of anthropogenic climate change documented in previous studies. By contrast, summer-rainfall and tundra climate zones show more heterogeneous patterns, with mixed streamflow trends but the strongest warming signal across all zones (+0.06 °C/year on average). In these regions, rising temperatures, snowmelt timing, and increased evapotranspiration appear to be increasingly essential controls on hydrological dynamics. Patagonian catchments display high spatial variability, reflecting the combined effects of westerly wind shifts, orography, and glacier dynamics.

Across all climate zones, accumulated precipitation emerges as the dominant control on streamflow variability, particularly in Mediterranean and temperate regions, where Spearman correlation coefficients range from $\rho=0.2$ to 0.79. Seven-day accumulated precipitation shows even stronger correlations in several catchments, highlighting the critical role of antecedent wetness conditions in runoff generation. Soil moisture acts as a key intermediate mechanism between precipitation and streamflow, especially in water-limited environments. Catchments with strong precipitation-soil moisture relationships also display strong soil moisture–streamflow coupling, reinforcing the conceptual model of soil moisture as a hydrological buffer that modulates precipitation–runoff transformation. This buffering effect has clear implications for drought propagation, as soil moisture deficits can amplify the hydrological impacts of precipitation anomalies. Temperature exhibits weaker direct correlations with annual maximum streamflow but exerts indirect influence through enhanced evapotranspiration and shifts in snowmelt timing, particularly in high-elevation Andean catchments. Together, declining precipitation and rising temperatures generate compounding stresses on water availability in central Chile.

The climate zone analysis reveals distinct response patterns. In Mediterranean regions, all hydro-climatic variables exhibit negative trends, and streamflow strongly reflects precipitation variability, making these catchments particularly vulnerable to



655

660

665

670

675

680



sustained drought. Temperate oceanic zones show the strongest precipitation—streamflow coupling, with soil moisture playing a clear intermediate role. Semi-arid zones exhibit weaker coupling and higher interannual variability, with temperature exerting a greater influence. In tundra regions, warming trends dominate and streamflow responses are more heterogeneous, reflecting the increasing importance of snow and glacier processes. Summer-rainfall regions are characterised by complex patterns influenced by ENSO variability, showing weaker long-term trends but high variability.

These findings advance our understanding of hydro-climatic interactions in several ways. First, integrating satellite soil moisture data with hydro-meteorological observations allows a more nuanced interpretation of precipitation—runoff processes, revealing how soil moisture modulates hydrological response and contributes to non-stationary runoff behaviour during droughts. Second, the comparative approach across multiple climate zones demonstrates that climate—streamflow relationships are spatially heterogeneous, underscoring the need for regionally tailored water management strategies rather than nationally uniform policies. Third, the trends quantified for the 2000–2021 period are consistent with longer-term observations and climate projections, providing a robust basis for assessing the impacts of anthropogenic climate change on Chilean hydrology.

These hydro-climatic changes have direct implications for water management. In Mediterranean and temperate regions, where the most severe declines were observed, immediate adaptation measures are required, including improved water storage, demand management, and drought preparedness. Snow-dominated Andean catchments are particularly vulnerable due to hydrological memory effects that amplify prolonged droughts, requiring strategies that address multi-year water deficits. Incorporating soil moisture monitoring into operational systems would provide valuable early warning information on catchment wetness conditions and drought propagation. Regional differentiation in management approaches is essential to account for the spatially diverse hydro-climatic responses observed across the country.

Future research should extend the temporal scope of analyses to include pre-2000 observations, enabling more precise separation of long-term climate change signals from natural multi-decadal variability. Attribution studies are also needed to disentangle the relative contributions of climatic drivers, land use change, and human water use. Process-based modelling could help better understand soil—atmosphere feedbacks, snow and glacier dynamics, and groundwater interactions. Moreover, sub-annual analyses could provide insight into shifts in streamflow timing and seasonality, while integration of climate projections would enable scenario-based assessment of future water availability.

In conclusion, the hydro-climatic assessment of 38 Chilean catchments over the past two decades reveals systematic streamflow declines in winter-rainfall regions primarily driven by reductions in precipitation, with soil moisture playing a key mediating role. The clear spatial contrasts in climate—streamflow relationships across Chile's diverse climatic zones underscore the complexity of hydrological responses to climate change and the necessity of region-specific management strategies. These





results contribute to the growing body of evidence documenting climate change impacts on water resources in Chile and provide a critical foundation for adaptive water governance in the coming decades.

Code availability. The codes used to develop all analyses and figures will be made available upon request.

690 Data availability. The CR2MET precipitation and temperature datasets (v2.5; 1960-2021) can be accessed at Zenodo (https://doi.org/10.5281/zenodo.7529681; Boisier, 2023) (last access: 24 July 2025). The DGA streamflow data was obtained at https://snia.mop.gob.cl/BNAConsultas/reportes (DGA, 2025) (last access: 24 July 2025). The NASA soil moisture data were GLDAS-2.1 obtained from the Noah model be accessed and can at https://disc.gsfc.nasa.gov/datasets/GLDAS NOAH025 3H 2.1/summary (Rodell et al. 2004) (last access: 24 July 2025).

Supplement. The supplement related to this article is available at supplement.

Author contributions.

695

Alejandra Stehr G.: Writing – original draft, Conceptualisation, Methodology, Formal analysis, Visualisation, Funding acquisition. Cristóbal Benavente.: Writing – original draft, Methodology, Formal analysis, Visualisation, Data curation. Felipe Orellana: Writing – review and editing, Methodology.

Competing interests. The authors declare that they have no conflicts of interest.

- Acknowledgements. We thank the Technische Universität Wien for their contributions to this work, specifically Dr Miriam Bertola. While preparing this work, the authors used ChatGPT, DeepL and Grammarly to improve language and readability. After using this tool, the authors reviewed and edited the content as needed and takes full responsibility for the content of the publication.
- 710 *Financial support.* This research has been supported by the Agencia Nacional de Investigación y Desarrollo (ANID, Chile) through the Programa de Investigación Asociativa Anillos (grant no. ATE220021, Climate change and the sociohydrology of floods, 2022–2025).

References

Alam, S., von Kaenel, M., Su, L., and Lettenmaier P.: The Role of Antecedent Winter Soil Moisture Carryover on Spring Runoff Predictability in Snow-Influenced Western U.S. Catchments, J. Hydrometeorol., 25, 1561-1575, https://doi.org/10.1175/JHM-D-24-0038.1, 2024.



735



- Alvarez-Garreton, C., Boisier, J. P., Garreaud R., Seibert, J., and Vis M.: Progressive water deficits during multi-year droughts in basins with long hydrological memory in Chile, Hydrol. Earth Syst. Sci., 25, 429–446, https://doi.org/10.5194/hess-25-429-2021, 2021.
- Al-Yaari, A., Ducharne, A., Cheruy, F., Crow, W. T., Wigneron, J.-P.: Satellite-based soil moisture provides missing link between summertime precipitation and surface temperature biases in CMIP5 simulations over conterminous United States.Sci Rep 9, 1657, https://doi.org/10.1038/s41598-018-38309-5, 2019.
 - Ashraf, M.S., Ahmad, I., Khan, N.M. Zhang, F., Bilal, A., and Guo, J.: Streamflow Variations in Monthly, Seasonal, Annual and Extreme Values Using Mann-Kendall, Spearmen's Rho and Innovative Trend Analysis, Water Resour. Manage., 35, 243–
- 725 261. https://doi.org/10.1007/s11269-020-02723-0, 2021.

https://doi.org/10.5194/egusphere-egu24-14621, 2024.

- Baez-Villanueva, O. M., Zambrano-Bigiarini, M., Miralles, D. G., Beck, H. E., Siegmund, J. F., Alvarez-Garreton, C., Verbist, K., Garreaud, R., Boisier, J. P., and Galleguillos, M.: On the timescale of drought indices for monitoring streamflow drought considering catchment hydrological regimes, Hydrol. Earth Syst. Sci., 28, 1415–1439, https://doi.org/10.5194/hess-28-1415-2024, 2024.
- Berghuijs, W. R., Harrigan, S., Molnar, P., Slater, L. J., and Kirchner, J. W.: The relative importance of different flood-generating mechanisms across Europe, Water Resour. Res., 55, 4582–4593, https://doi.org/10.1029/2019WR024841, 2019.
 Bhatti, A. S., Hagan, D. F. T., Wang, G., Ullah, W., Ullah, S., Nooni, I. K., Amankwah, S. O. Y., and Zhou, F.: Unraveling the Complex Causal Relationship between Soil Moisture and Air Temperature Anomalies: A Comparative Analysis of Linear and Non-linear Granger Causality, EGU General Assembly 2024, Vienna, Austria, 14–19 Apr 2024, EGU24-14621,
- Blöschl, G., Hall, J., Viglione, A., Perdigão, R. A. P., Parajka, J., Merz, B., Lun, D., Arheimer, B., Aronica, G. T., Bilibashi, A., Boháč, M., Bonacci, O., Borga, M., Čanjevac, I., Castellarin, A., Chirico, G. B., Claps, P., Frolova, N., Ganora, D., Gorbachova, L., Gül, A., Hannaford, J., Harrigan, S., Kireeva, M., Kiss, A., Kjeldsen, T. R., Kohnová, S., Koskela, J. J., Ledvinka, O., Macdonald, N., Mavrova-Guirguinova, M., Mediero, L., Merz, R., Molnar, P., Montanari, A., Murphy, C.,
- Osuch, M., Ovcharuk, V., Radevski, I., Salinas, J. L., Sauquet, E., Šraj, M., Szolgay, J., Volpi, E., Wilson, D., Zaimi, K., and Živković, N.: Changing climate both increases and decreases European river floods, Nat., 573, 108–111, https://doi.org/10.1038/s41586-019-1495-6, 2019.
 - Boisier, J. P.: CR2MET: A high-resolution precipitation and temperature dataset for the period 1960-2021 in continental Chile. (v2.5), Zenodo [data set], https://doi.org/10.5281/zenodo.7529682, 2023.
- Poisier, J. P., Alvarez-Garretón, C., Cordero, R. R., Damiani, A., Gallardo, L., Garreaud, R. D., Lambert, F., Ramallo, C., Rojas, M., and Rondanelli, R.: Anthropogenic drying in central-southern Chile evidenced by long-term observations and climate model simulations, Elem. Sci. Anth., 6, 74, https://doi.org/10.1525/elementa.328, 2018.
 - Crameri, F., Shephard, G. E., and Heron, P. J.: The misuse of colour in science communication, Nat. Commun, 11, 5444, https://doi.org/10.1038/s41467-020-19160-7, 2020.



765



- Crosbie, R. S., Scanlon, B. R., Mpelasoka, F. S., Reedy, R. C., Gates, J. B., and Zhang, L.: Potential climate change effects on groundwater recharge in the High Plains aquifer, USA, Water Resour. Res., 49, 3936–3951, https://doi.org/10.1002/wrcr.20292, 2013.
 - Dirección General de Aguas (DGA): Streamflow data from Chilean hydrometric stations: https://snia.mop.gob.cl/BNAConsultas/reportes, last access: 24 Jul 2024.
- Do, H. X., Westra, S., and Leonard, M.: A global-scale investigation of trends in annual maximum streamflow, J. Hydrol., 552, 28-43, https://doi.org/10.1016/j.jhydrol.2017.06.015, 2017.
 - Falvey, M. and Garreaud, R. D.: The Andes climate and weather, Adv. Geosci., 22, 3–11, doi:10.5194/adgeo-22-3-2009, 2009. Gentilucci, M., Djouohou, S.I., Barbieri, M., Hamed, Y., and Pambianchi, G.: Trend Analysis of Streamflows in Relation to Precipitation: A Case Study in Central Italy, Water, 15, 1586. https://doi.org/10.3390/w15081586, 2023.
- Giuntoli, I., Renard, B., Vidal, J. P., and Bard, A.: Low flows in France and their relationship to large-scale climate indices, J. Hydrol., 482, 105–118, https://doi.org/10.1016/j.jhydrol.2012.12.038, 2013.
 - Goddard Earth Sciences Data and Information Services Center (NASA GES DISC): GLDAS-2.1 Noah Land Surface Model data: https://disc.gsfc.nasa.gov/datasets/GLDAS NOAH025 3H 2.1/summary, last access: 24 July 2025.
 - Gocic, M., and Trajkovic, S.: Analysis of changes in meteorological variables using Mann-Kendall and Sen's slope estimator statistical tests in Serbia, Glob. Planet. Chang., 100, 172–182, https://doi.org/10.1016/j.gloplacha.2012.10.014, 2013.
 - Gudmundsson, L., Tallaksen, L. M., and Stahl, K.: Spatial cross-correlation patterns of European low, mean and high flows, Hydrol. Process., 25, 1034–1049, https://doi.org/10.1002/hyp.7807, 2011.
 - Hasson, S., Böhner, J., and Lucarini, V.: Prevailing climatic trends and runoff response from Hindukush–Karakoram–Himalaya, upper Indus Basin, Earth Syst. Dynam., 8, 337–355, https://doi.org/10.5194/esd-8-337-2017, 2017.
- IPCC: Climate Change 2023: Synthesis Report. Contribution of Working Groups I, II and III to the Sixth Assessment Report of the Intergovernmental Panel on Climate Change [Core Writing Team, H. Lee and J. Romero (eds.)], IPCC, Geneva, Switzerland, https://doi.org/10.59327/IPCC/AR6-9789291691647, 2023.
 - Kendall, M. G.: Rank Correlation Methods, 4th edn., Charles Griffin, London, 202 pp., ISBN 0852641990, 1975.
- Lu, Z., Zhang, J., Li, C., Wang, X., Lei, G., and Li, K.: Modeling hydrological processes and analysing water balance utilising remote sensing data and physical hydrological models in the Songnen Plain, China, PLoS One, 20, e0329816, https://doi.org/10.1371/journal.pone.0329816, 2025.
 - Madariaga Gomez de Cuenca, M.: Is Chile building good climate governance? Reflections on the drafting process of the climate change framework law, Environ. Law Rev., 23(1), 40-48, https://doi.org/10.1177/1461452920985654, 2021.
 - Mann, H. B.: Non-parametric tests against trend, Econometrica, 13, 245-259, https://doi.org/10.2307/1907187, 1945.
- Mediero, L., Santillán, D., Garrote, L., and Granados, A.: Detection and attribution of trends in magnitude, frequency and timing of floods in Spain, J. Hydrol., 517, 1072–1088, https://doi.org/10.1016/j.jhydrol.2014.06.040, 2014.





- Minaei, M., and Irannezhad, M.: Spatio-temporal trend analysis of precipitation, temperature, and river discharge in the northeast of Iran in recent decades, Theor. Appl. Climatol., 131, 167–179, https://doi.org/10.1007/s00704-016-1963-y, 2018.
- Miranda, A., Altamirano, A., Cayuela, L., Lara, A., Gonzalez, M.: Native forest loss in the Chilean biodiversity hotspot: revealing the evidence, Reg Environ Change, 17. 285-297, https://doi.org/10.1007/s10113-016-1010-7, 2017.
 - Myronidis, D., Ioannou, K., Fotakis, D., and Dörglinger, G.: Streamflow and Hydrological Drought Trend Analysis and Forecasting in Cyprus, Water Resour. Manage., 32, 1759–1776, https://doi.org/10.1007/s11269-018-1902-z, 2018.
 - Oertel, M., Meza, F. J., Gironás, J.: Observed trends and relationships between ENSO and standardised hydro-meteorological drought indices in central Chile, 34, 159-174, https://doi.org/10.1002/hyp.13596, 2020.
- Rodell, M., Houser, P. R., Jambor, U., Gottschalck, J., Mitchell, K., Meng, C.-J., Arsenault, K., Cosgrove, B., Radakovich, J., Bosilovich, M., Entin, J.K., Walker, J.P., Lohmann, D., and Toll, D.: The Global Land Data Assimilation System, Bull. Amer. Meteor. Soc., 85, 381-394, https://doi.org/10.1175/BAMS-85-3-381, 2004.
 - Salazar, Á., Thatcher, M., Goubanova, K., Bernal, P., Gutiérrez, J., and Squeo, F.: CMIP6 precipitation and temperature projections for Chile, Clim. Dyn., 62, 2475–2498, https://doi.org/10.1007/s00382-023-07034-9, 2024.
- Sangüesa, C., Pizarro, R., Ingram, B., Balocchi, F., García-Chevesich, P., Pino, J., Ibáñez, A., Vallejos, C., Mendoza, R., Bernal, A., Valdés-Pineda, R., and Pérez, F.: Streamflow Trends in Central Chile, Hydrol., 10, 144. https://doi.org/10.3390/hydrology10070144, 2023.
 - Sarricolea, P., Herrera-Ossandon, M. J., and Meseguer-Ruiz, Ó.: Climatic regionalisation of continental Chile, J. Maps, 13, 66-73, https://doi.org/10.1080/17445647.2016.1259592, 2017.
- 800 Sen, P. K.: Estimates of the regression coefficient based on Kendall's tau, J. Am. Stat. Assoc., 63, 1379–1389, https://doi.org/10.1080/01621459.1968.10480934, 1968.
 - Spearman, C.: The proof and measurement of association between two things, Am. J. Psychol., 15, 72–101, https://doi.org/10.2307/1412159, 1904.
- Stolpe, N., and Undurraga, P.: Long term climatic trends in Chile and effects on soil moisture and temperature regimes, Chilean J. Agric. Res., 76, 487-496, http://dx.doi.org/10.4067/S0718-58392016000400013, 2016.
 - Swain, S. S., Mishra, A., and Chatterjee, C.: Time-Varying Evaluation of Compound Drought and Hot Extremes in Machine Learning–Predicted Ensemble CMIP5 Future Climate: A Multivariate Multi-Index Approach, J. Hydrol. Eng., 29, 06024006, https://doi.org/10.1061/JHYEFF.HEENG-6026, 2024.
- Theil, H.: A rank-invariant method of linear and polynomial regression analysis, I, II, and III, Nederl. Akad. Wetensch. Proc., 810 53, 386–392, 521–525, 1397–1412, 1950.
 - Vásquez, N. A., Mendoza, P. A., Lagos-Zuñiga, M., Scaff, L., Muñoz-Castro, E., and Vargas, X.: Robust spatial changes in climate classes: insights from bias-corrected CMIP6 models across Chile, Environ. Res. Lett., 20, 014061, 10.1088/1748-9326/ad9d5b, 2024.



830



- Vicente, G. A.: Tools and Data Services from the NASA Earth Satellite Observations for Climate Applications, in: Proceedings of the EUMETSAT Meteorological Satellite Conference 2005, Dubrovnik, Croatia, 19–23 September 2005, NASA Goddard Space Flight Center, https://ntrs.nasa.gov/api/citations/20060002809/downloads/20060002809.pdf, 2005.
 - Vicuña, S., Gironás, J., Meza, F. J., Cruzat, M. L., Jelinek, M., Bustos, E., Poblete, D., and Bambach, N., (2013) Exploring possible connections between hydrological extreme events and climate change in central south Chile, Hydrol. Sci. J., 5, 1598-1619, 10.1080/02626667.2013.840380, 2013.
- Viviroli, D., Archer, D. R., Buytaert, W., Fowler, H. J., Greenwood, G. B., Hamlet, A. F., Huang, Y., Koboltschnig, G., Litaor, M. I., López-Moreno, J. I., Lorentz, S., Schädler, B., Schreier, H., Schwaiger, K., Vuille, M., and Woods, R.: Climate change and mountain water resources: overview and recommendations for research, management and policy, Hydrol. Earth Syst. Sci., 15, 471–504, https://doi.org/10.5194/hess-15-471-2011, 2011.
- Wan, N., Lin, X., Pielke Sr., R. A., Zeng, X., and Nelson, A. M.: Global total precipitable water variations and trends over the period 1958–2021, Hydrol. Earth Syst. Sci., 28, 2123–2137, https://doi.org/10.5194/hess-28-2123-2024, 2024.
 - Wasko, C. and Nathan, R.: Influence of changes in rainfall and soil moisture on trends in flooding, J. Hydrol., 575, 432–441, https://doi.org/10.1016/j.jhydrol.2019.05.054, 2019.
 - Xu, R., Qiu, D., Gao, P., Wu, C., Mu, X., and Ismail, M., Prediction of streamflow based on the long-term response of streamflow to climatic factors in the source region of the Yellow River, J. Hydrol.: Reg. Stud., 52, 101681, https://doi.org/10.1016/j.eirh.2024.101681, 2024.
 - Yest, P., Dorador, J., Martin-Rosale, W., Molero, E., Esteban-Parra, M. J., and Rueda, F. J., Climate-driven trends in the streamflow records of a reference hydrologic network in Southern Spain, J. Hydrol., 566, 55-72, https://doi.org/10.1016/j.jhydrol.2018.08.063, 2018.
- Zhai, R. and Tao, F.: Contributions of climate change and human activities to runoff changes in seven typical catchments across China, Sci. Total Environ., 605–606, 219–229, https://doi.org/10.1016/j.scitotenv.2017.06.210, 2017.
 - Zhang, Q., Sun, P., Singh, V. P., and Chen, X.: Spatial-temporal precipitation changes (1956–2000) and their implications for agriculture in China, Global Planet. Change, 82-83, 86-95, https://doi.org/10.1016/j.gloplacha.2011.12.001, 2012.